Elementary theory of bed-sediment entrainment by debris flows and avalanches

Richard M. Iverson[1]

Received 11 August 2011; revised 15 May 2012; accepted 16 May 2012; published 19 July 2012.

[1] Analyses of mass and momentum exchange between a debris flow or avalanche and an underlying sediment layer aid interpretations and predictions of bed-sediment entrainment rates. A preliminary analysis assesses the behavior of a Coulomb slide block that entrains bed material as it descends a uniform slope. The analysis demonstrates that the block's momentum can grow unstably, even in the presence of limited entrainment efficiency. A more-detailed, depth-integrated continuum analysis of interacting, deformable bodies identifies mechanical controls on entrainment efficiency, and shows that entrainment rates satisfy a jump condition that involves shear-traction and velocity discontinuities at the flow-bed boundary. Explicit predictions of the entrainment rate E result from making reasonable assumptions about flow velocity profiles and boundary shear tractions. For Coulomb-friction tractions, predicted entrainment rates are sensitive to pore fluid pressures that develop in bed sediment as it is overridden. In the simplest scenario the bed sediment liquefies completely, and the entrainment-rate equation reduces to $E = 2\mu_1 g h_1 \cos\theta(1-\lambda_1)/\bar{v}_1$, where θ is the slope angle, μ_1 is the flow's Coulomb friction coefficient, h_1 is its thickness, λ_1 is its degree of liquefaction, and $\bar{v}_1$ is its depth-averaged velocity. For values of λ_1 ranging from 0.5 to 0.8, this equation predicts entrainment rates consistent with rates of 0.05 to 0.1 m/s measured in large-scale debris-flow experiments in which wet sediment beds liquefied almost completely. The propensity for bed liquefaction depends on several factors, including sediment porosity, permeability, and thickness, and rates of compression and shear deformation that occur when beds are overridden.

Citation: Iverson, R. M. (2012), Elementary theory of bed-sediment entrainment by debris flows and avalanches, *J. Geophys. Res.*, *117*, F03006, doi:10.1029/2011JF002189.

1. Introduction

[2] Researchers have long recognized that debris flows and avalanches can gain much of their mass and destructive power by entraining material as they descend steep slopes and channels [e.g., *Stiny*, 1910; *Heim*, 1932; *Takahashi*, 1978, 1991; *Hungr et al.*, 1984, 2005]. Entrainment is defined in this paper as incorporation of solid and fluid boundary material that does not appreciably change the bulk composition of a flow, whereas bulking is defined as incorporation of material that increases a flow's solid volume fraction [e.g., *Scott et al.*, 2005; *Fagents and Baloga*, 2006; *Berzi et al.*, 2010; *Doyle et al.*, 2011]. Entrainment can result from scour of bed material or collapse of channel banks, and it can cause flow mass to grow many-fold before deposition begins on flatter terrain downstream [e.g., *Pierson*, 1980; *Benda*, 1990; *Pierson et al.*, 1990; *Berti et al.*, 1999; *Wang et al.*, 2003; *Godt and Coe*, 2007; *Breien et al.*, 2008]. In this paper, deposition is treated as negative entrainment.

[3] Diverse field and laboratory studies have assessed bed-sediment entrainment by debris flows and avalanches [e.g., *Sassa*, 1985; *Voight and Sousa*, 1994; *Abele*, 1997; *Egashira et al.*, 2001; *Rickenmann et al.*, 2003; *Hungr and Evans*, 2004; *Papa et al.*, 2004; *Berger et al.*, 2011; *Mangeney et al.*, 2010; *Iverson et al.*, 2011; *Reid et al.*, 2011; S. W. McCoy et al., Sediment entrainment by debris flows: In situ measurements from the headwaters of a small catchment, submitted to *Journal of Geophysical Research*, 2012], and diverse numerical models have included entrainment terms in simulations of evolving flow behavior [e.g., *Brufau et al.*, 2000; *Pitman et al.*, 2003; *McDougall and Hungr*, 2005; *Chen et al.*, 2006; *Mangeney et al.*, 2007; *Tai and Kuo*, 2008; *Bouchut et al.*, 2008; *Armanini et al.*, 2009; *Crosta et al.*, 2009a; *Le and Pitman*, 2010]. Nevertheless, as summarized by *Hungr and Evans* [2004] and *Bouchut et al.* [2008], the theoretical basis for evaluating entrainment rates has remained tenuous. Consequently, models of debris-flow and avalanche dynamics typically have excluded the effects of entrainment [e.g., *Denlinger and Iverson*, 2001, 2004] or have relied on ad hoc rules or empirical calibrations to evaluate entrainment terms [e.g., *McDougall and Hungr*, 2005; *Armanini et al.*, 2009].

[4] Here, to aid mechanistic prediction and interpretation of bed-sediment entrainment, I analyze the phenomenon in two ways. First I present a heuristic slide-block model aimed

[1]U.S. Geological Survey, Vancouver, Washington, USA.

Corresponding author: R. M. Iverson, U.S. Geological Survey, 1300 SE Cardinal Ct., Vancouver, WA 98683, USA.

This paper is not subject to U.S. copyright.
Published in 2012 by the American Geophysical Union.

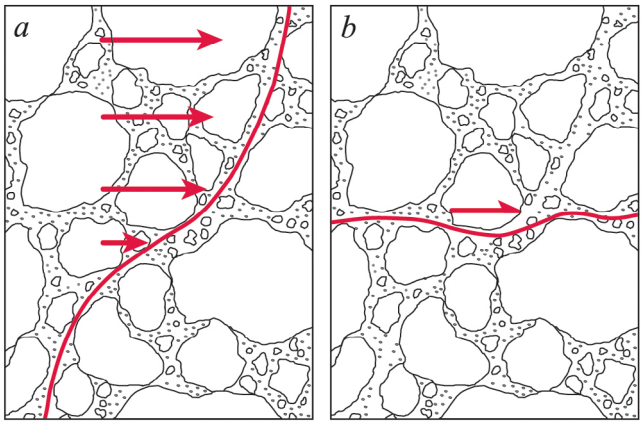

Figure 1. Schematic vertical cross-sectional views of shear deformation that might occur as a flow of poorly sorted debris interacts with entrainable bed material. Red curves and arrows depict alternative views of the same deformation. (a) Viewed at the scale of the smallest grains, shear deformation is distributed in a zone of finite thickness. (b) Viewed at a scale exceeding that of the largest grains, shear deformation is focused along a discrete slip surface.

at clarifying the role that bed-sediment inertia and entrainment efficiency play when slide-block mass and momentum evolve simultaneously. I then formulate a three-layer, depth-integrated, continuum-mechanical model of mass and momentum exchange between a flow, an erodible bed, and a stable substrate. A depth-integrated approach has inherent limitations, but it holds some advantages over more-detailed approaches because it combines the effects of boundary conditions, mass fluxes, and momentum fluxes into conservation equations that encapsulate the mechanics of individual layers as well as the three-layer system as a whole. A depth-integrated analysis also facilitates evaluation of jump discontinuities, which play a crucial role at the interfaces between adjacent layers.

[5] New analyses of the entrainment process are warranted in view of results of recent field and laboratory studies, which have demonstrated that entrainment beneath debris flows and avalanches generally occurs by progressive scour rather than mass failure of bed material [*Mangeney et al.*, 2010; *Berger et al.*, 2011; *Iverson et al.*, 2011; *Reid et al.*, 2011; McCoy et al., submitted manuscript, 2012]. The latter three studies have additionally shown that entrainment rates are sensitive to pore fluid pressures that develop in bed sediment as it is overridden. Thus, a primary goal of the analyses here is to provide a theoretical basis for interpreting and predicting factors that determine entrainment rates and their dependence on pore pressures and effective-stress states in bed sediment. A secondary goal, which cannot be separated from the first, is to assess coupling between entrainment and flow dynamics.

2. Entrainment Velocity

[6] Neither of the analyses presented here considers detailed, grain-scale mechanics, but both analyses include constraints imposed by momentum conservation as the bed exchanges arbitrarily small elements of mass with the overriding flow. By definition, these elements of bed material must attain the basal flow velocity in order to be entrained [cf. *Gray*, 2001]. In this context "erosion," "scour," and "entrainment" are synonymous, because the analyses assume that material along the flow-bed interface has little or no velocity before it is entrained, and has the basal flow velocity after it is entrained. Intermediate velocities necessarily occur as small elements of bed material accelerate to merge with the flow, but they cannot be resolved by slide-block or depth-integrated continuum analyses.

[7] The presence of an erodible bed can make basal slip velocities difficult to assess because the location of the boundary between the flow and bed may be indistinct – as documented for idealized flows of nearly identical grains [*Komatsu et al.*, 2001; *Armanini et al.*, 2005; *Larcher et al.*, 2007; *Crosta et al.*, 2009b]. For flows of poorly sorted geological debris, however, distinctions between infinitesimal and finite slip velocities can hinge largely on the scale at which the flow-bed interface is observed (Figure 1). For example, continuum-scale velocity fields constructed using measured trajectories of large particles in experimental debris flows indicate that the flows have finite basal slip velocities [*Johnson et al.*, 2012]. From this perspective entrainment analyses that consider the role of finite basal slip velocities appear appropriate. Such analyses also demonstrate that entrainment-rate data, interpreted in the context of momentum conservation and bed stress states, can help constrain basal slip velocities when they are not directly observable.

3. Slide-Block Analysis

[8] This analysis considers behavior of a single body (i.e., a slide block) that encompasses all mass in motion as the block descends a slope covered with entrainable bed material. By definition, the evolving block mass includes material actively undergoing entrainment, but does not include bed material prior to the onset of its entrainment (Figure 2). This

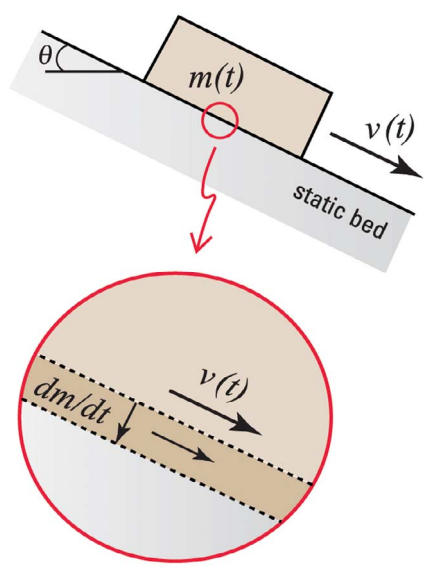

Figure 2. Schematic illustration of a Coulomb slide block of mass $m(t)$ and velocity $v(t)$ descending a plane inclined at the angle θ. Expanded view shows that the block gains mass at a rate dm/dt by exerting a basal force that accelerates static bed material.

definition precludes analysis of the behavior of slide blocks that lose mass through deposition, as clarified below.

[9] Newton's second law states that the evolving slide-block momentum obeys

$$\frac{d(mv)}{dt} = F, \tag{1}$$

where t is time, m is the slide-block mass, v is its velocity, and F is the sum of external forces acting on the block. If the block descends a plane inclined at a uniform angle θ, and its descent is resisted by basal Coulomb friction characterized by a friction coefficient μ, then F is given by

$$F = mg', \tag{2}$$

where

$$g' = g(\sin\theta - \mu\cos\theta) \tag{3}$$

summarizes the net effect of gravitational acceleration, g. The net force F can be represented as $F = mg'$ because, like the gravitational driving force, the Coulomb friction force is proportional to mg.

[10] Use of a Coulomb friction rule for bed sediment undergoing entrainment assumes that the sediment immediately beneath the slide block attains a state of limiting equilibrium before entrainment begins. Gravity suffices to produce this limiting equilibrium state if θ equals the sediment's angle of repose. If θ is less than the angle of repose, a limit-equilibrium state can result from reduction of frictional resistance that occurs as the slide block overrides the bed [cf. *Mangeney et al.*, 2007]. Such a reduction might be caused by bed deformation that increases pore fluid pressure and thereby reduces the effect of $mg\ \mu\cos\theta$, for example [e.g., *Hungr and Evans*, 2004]. Modeling pore pressure effects on bed-sediment resistance is beyond the scope of the slide-block analysis, but is emphasized in the continuum-mechanical analysis that follows.

[11] Coulomb friction coefficients for landslides, debris flows, and bed sediment are commonly assumed to be constant, and constant friction represents an important baseline case. On the other hand, evidence from diverse experiments with dense grain flows and grain-fluid suspensions indicates that Coulomb friction increases systematically as the shear rate increases [e.g., *MiDi GDR Group*, 2004; *Forterre and Pouliquen*, 2008; *Boyer et al.*, 2011]. This shear-rate effect cannot be fully incorporated in a slide-block model, but it can be represented in a rudimentary way by expressing the basal friction coefficient as the sum of a constant component μ_0 and a velocity-dependent component $\mu_V(v/V)$,

$$\mu = \mu_0 + \mu_V\frac{v}{V}, \tag{4}$$

where μ_V and V are constants. More specifically, V is a velocity scale quantified in the analysis that follows.

[12] Substituting (2), (3), and (4) into (1) yields a slide-block momentum equation that can be written as

$$m\frac{dv}{dt} = m(G - \Gamma v) - v\frac{dm}{dt}, \tag{5}$$

where the forcing terms on the right–hand side include constants defined as

$$G = g(\sin\theta - \mu_0\cos\theta), \tag{6}$$

$$\Gamma = g\mu_V\cos\theta/V. \tag{7}$$

The term $-v(dm/dt)$ arises in (5) as a consequence of momentum conservation, but it can be interpreted more precisely as the reaction force experienced by the slide block as it exerts force to overcome the inertia of static bed material while accelerating that material to the ambient block velocity v. This effect of inertia constitutes an internal force because the slide-block definition includes all material in motion. By contrast, the action of an additional external force (i.e., a resistive force exerted by stationary bed material) would be required to cause deposition of basal slide-block material (i.e., $dm/dt < 0$). Such externally driven mass loss differs fundamentally from internally driven mass loss that occurs when a rocket forcibly ejects matter to propel itself [*Hungr*, 1990; *Erlichson*, 1991]. As a result, "rocket equations" similar to (5) are inappropriate for analyzing motion of debris flows or avalanches that lose mass through deposition [cf. *Cannon and Savage*, 1988; *Van Gassen and Cruden*, 1989].

[13] The physical implications of (5) can be investigated by first considering some special cases in which constraints are placed on m and/or v. For example, if $dm/dt = 0$, then the entire net driving force $m(G - \Gamma v)$ causes slide-block acceleration, and (5) has solutions that describe maximum velocities attainable by slide blocks at any particular time. For the initial condition $v = v_0$, one of these solutions applies if friction is exclusively rate-independent (i.e., $\Gamma = 0$):

$$\frac{v}{v_0} = 1 + \frac{Gt}{v_0}. \tag{8}$$

Another solution applies if rate-independent and rate-dependent friction coexist:

$$\frac{v}{v_0} = \frac{G}{\Gamma v_0} + \left(1 - \frac{G}{\Gamma v_0}\right)\exp(-\Gamma t). \tag{9}$$

Whereas (8) indicates that the slide-block velocity increases constantly, (9) shows that rate-dependent friction causes the velocity to asymptotically approach the steady state $v = G/\Gamma$. A fixed fraction of G/Γ is therefore a logical choice for the velocity scale V in (4) and (7).

[14] In more-general cases with $dm/dt > 0$, the slide-block behavior described by (5) can be more complex. The implications of dm/dt can be identified most readily by first rewriting (5) as

$$\frac{dm}{dt} = \frac{m}{v}[G - \Gamma v - (dv/dt)]. \tag{10}$$

If the block velocity is constant ($v = v_0$ and $dv/dt = 0$) and the initial condition is $m = m_0$, then the solution of (10) shows that m grows exponentially:

$$\frac{m}{m_0} = \exp\left[\left(\frac{G - \Gamma v_0}{v_0}\right)t\right]. \tag{11}$$

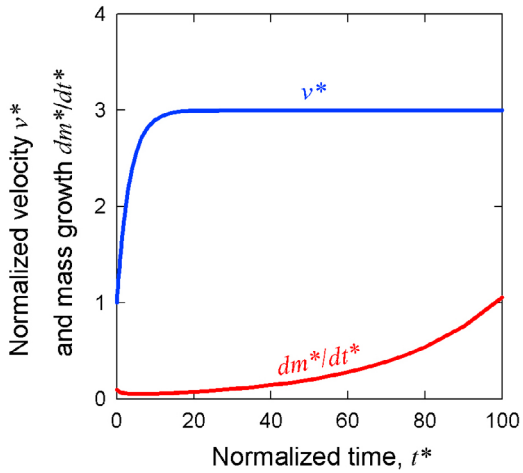

Figure 3. Graphs of slide-block behavior represented by equations (16) and (17) with parameter values $\alpha = 0.1$ and $\Gamma v_0/G = 0.3$. Here normalized time is defined as $t^* = tG/v_0$, normalized velocity is defined as $v^* = v/v_0$, and normalized mass is defined as $m^* = m/m_0$.

This unbounded growth of m occurs in the presence of a constant v because the entire net force $F = m(G - \Gamma v_0)$ acts to cause entrainment, while the net force itself grows in proportion to m.

[15] The behavior described by (11) reveals a fundamental asymmetry in the dynamics of Coulomb slide blocks entraining mass: a constant m implies stable growth of v, as described by (8) and (9), whereas a constant v implies unstable growth of m. (The mathematically stable case with $\Gamma > G/v_0$ in (11) lacks physical relevance because it implies that mass loss occurs, violating the assumptions used to derive (5)). Equation (11) also demonstrates that a constant slide-block velocity cannot be accompanied by a constant dm/dt. Thus, no physically valid entrainment rule can have the seemingly plausible form $dm/dt \propto v$.

[16] On the other hand, equations (10) and (11) provide a basis for proposing an entrainment formula in which $dm/dt \propto m/v$. The basis is established by first considering an ideal case in which frictional resistance is zero (i.e., $G = G_0 = g \sin\theta$, $\Gamma = 0$) and the driving force $F = mG_0$ is allocated entirely to entrainment, implying that v is constant. Then (10) reduces to

$$\left[\frac{dm}{dt}\right]_{\max} = G_0 \frac{m}{v_0}, \tag{12}$$

where $[dm/dt]_{\max}$ is the maximum entrainment rate that can occur without causing deceleration and eventual stoppage of the slide block. Because (12) describes an upper-bound condition for sustainable entrainment, it is reasonable to postulate that a more-general entrainment formula can have the analogous form

$$\frac{dm}{dt} = \alpha G \frac{m}{v}, \tag{13}$$

where α is an entrainment-efficiency parameter. The value of α must satisfy $0 \le \alpha \le 1$, but it need not be constant. Indeed, if the value of α evolves so that it always obeys $\alpha = 1 - [(dv/dt + \Gamma v)/G]$, then (13) simply restates (5), resulting in indeterminate behavior.

[17] Although a constant α is not mandatory, the behavior of slide blocks with constant entrainment efficiency is instructive. This behavior can be clarified by finding solutions of the two-equation system, (5) and (13), for cases in which α is constant. One solution applies if friction has no rate-dependence (i.e., $\Gamma = 0$):

$$\frac{v}{v_0} = 1 + \frac{(1-\alpha)Gt}{v_0}, \tag{14}$$

$$\frac{m}{m_0} = \left[\frac{v}{v_0}\right]^{\frac{\alpha}{1-\alpha}} = \exp\left(\frac{\alpha}{1-\alpha}[\ln(v/v_0)]\right). \tag{15}$$

In this case α regulates slide-block velocity and mass growth in a straightforward way. If $\alpha = 1/2$, for example, normalized values of v and m grow at identical linear rates: $v/v_0 = m/m_0 = 1 + (Gt/2v_0)$. In this special case the net driving force is allocated equally between the two growth phenomena. In general, however, equal force allocation is unnecessary, and balanced growth of v and m does not occur. For $\alpha < 1/2$, linear growth of v outpaces nonlinear growth of m, whereas the opposite is true for $\alpha > 1/2$. If $\alpha \to 1$, then $m \to \infty$, and this singular behavior reinforces the evidence of instability expressed by (11).

[18] A different solution of (5) and (13) applies if α is constant and rate-dependent friction exists ($\Gamma > 0$):

$$\frac{v}{v_0} = \frac{(1-\alpha)G}{\Gamma v_0} + \left(1 - \frac{(1-\alpha)G}{\Gamma v_0}\right)\exp(-\Gamma t), \tag{16}$$

$$\frac{m}{m_0} = \left[\frac{v}{v_0}\right]^{\frac{\alpha}{1-\alpha}} \exp\left(\frac{\alpha \Gamma t}{1-\alpha}\right) = \exp\left(\frac{\alpha}{1-\alpha}[\ln(v/v_0) + \Gamma t]\right). \tag{17}$$

This solution indicates that exponential growth of m is inevitable for any nonzero value of α. Physically, this behavior results from v approaching the steady state $v = (1-\alpha)G/\Gamma$, implying that an increasing percentage of the net driving force is allocated to mass growth. Therefore, somewhat paradoxically, velocity stabilization by rate-dependent friction exerts a destabilizing effect on mass and momentum growth. For small values of α and Γ, however, a seemingly stable near-balance between the slide-block velocity and entrainment rate can persist for a considerable time before conspicuous acceleration of mass growth begins (Figure 3). This behavior temporarily mimics that of an equilibrium relationship between v and dm/dt, although no true equilibrium is possible.

[19] Despite its simplicity, the slide-block analysis illustrates several important principles that apply to motion and mass entrainment resisted by rate-independent and/or rate-dependent Coulomb friction. Perhaps the most fundamental principle is that bed-sediment inertia produces an inverse relationship between the slide-block velocity and mass-entrainment rate, if all other factors are equal. Subsequent

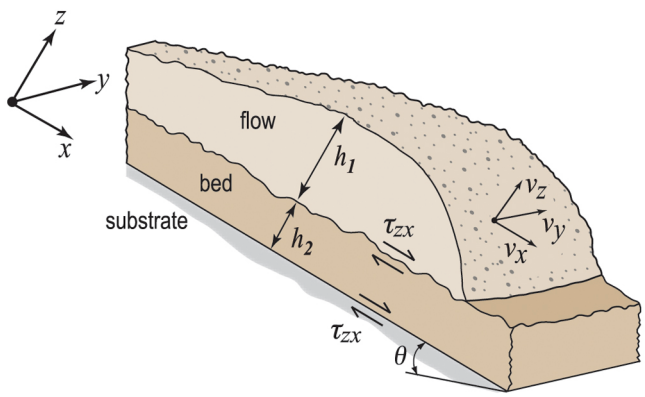

Figure 4. Schematic cutaway view of a debris flow or avalanche crossing a nearly tabular, erodible sediment bed overlying a strong substrate inclined at the angle θ. A Cartesian coordinate system used to analyze the flow is oriented such that x points down the fall line and z points upward, normal to x.

sections of the paper present a continuum mechanical analysis that reinforces this principle and also demonstrates how boundary shear tractions influence the entrainment efficiency parameterized above by α.

4. Depth-Integrated Continuum Analysis

[20] A more-thorough analysis considers mass and momentum exchange between three continuous layers, one representing a flow with a free upper surface, one representing an entrainable bed-sediment layer, and one representing a deeper substrate that cannot be entrained owing to its high strength (Figure 4). This configuration is similar to that of large-scale entrainment experiments involving tabular layers of nearly homogeneous sediment on a uniform, concrete slope [*Iverson et al.*, 2011; *Reid et al.*, 2011]. The analysis employs a Cartesian coordinate system in which x points in the downslope direction, y points in the cross-slope direction, and z points upward, normal to the slope. To emphasize essential mechanical principles and minimize mathematical complexity, it assumes that variations of all quantities in the y direction are negligible, and that temporal and spatial variations of the bulk density ρ of the flow and bed material are negligible. A derivation of the depth-integrated balance equations used in the analysis shows how the effects of these variations can be included, however (Appendix A).

[21] Like most depth-integrated theories, the analysis assumes that the z-momentum balance everywhere reduces to an equation describing one-dimensional static equilibrium,

$$\partial\sigma_{zz}/\partial z = -\rho g \cos\theta, \tag{18}$$

where σ_{zz} is the z-direction total normal stress (reckoned positive in compression), g is the magnitude of gravitational acceleration, and θ is the slope angle. Treatment of the z-momentum balance in such a simple way may be inappropriate in some instances, particularly if flows traverse irregular terrain [*Denlinger and Iverson*, 2004]. Here, however, this simplification sharpens the focus of the analysis by isolating the effects of the x momentum component on entrainment.

4.1. Balance Equations for Individual Layers

[22] Under the assumptions summarized above, the depth-integrated mass balance and x-momentum balance for each layer reduce to (Appendix A):

$$\frac{\partial h}{\partial t} + \frac{\partial(h\bar{v})}{\partial x} = -E_{top} + E_{bot} \tag{19}$$

$$\rho\left[\frac{\partial(h\bar{v})}{\partial t} + \frac{\partial(\beta h\bar{v}^2)}{\partial x}\right] = \int_{z_{bot}}^{z_{top}} \Sigma F dz - \rho v_{top}E_{top} + \rho v_{bot}E_{bot} \tag{20}$$

where h is the layer thickness in the z direction, $\bar{v}$ is the depth-averaged velocity of the layer, ΣF is the sum of external forces per unit volume acting on the layer, and the subscripts *top* and *bot* denote the upper and lower boundaries of the layer, respectively. In (19) E_{top} and E_{bot} describe z-direction boundary-migration rates caused by transfer of mass through the upper or lower boundary. At each location E is reckoned positive downward in order to emphasize boundary migration that occurs during bed-sediment entrainment by an overriding layer. In (20) the boundary momentum-flux terms $-\rho v_{top}E_{top}$ and $\rho v_{bot}E_{bot}$ arise mathematically from use of the mass-conservation equation during depth integration of the momentum-conservation equation (Appendix A). Physically, these momentum-flux terms account for the possibility that mass entering a layer through its boundary has a nonzero x-velocity component (v_{top} or v_{bot}), and thereby transfers some x-momentum with it. Of course, momentum must be conserved during such a transfer – a matter addressed below by considering interactions between adjacent layers.

[23] Equation (20) also contains a Boussinesq momentum-distribution coefficient, β, which accounts for the effects of nonuniform advection of x-momentum as a function of z within each layer. The coefficient is defined mathematically by

$$\beta = \frac{1}{h\bar{v}^2}\int_{z_{bot}}^{z_{top}} v^2 dz \tag{21}$$

where v is the local x-velocity component. Values of β determined from (21) range from $\beta = 1$ for a flow with all motion concentrated as basal slip to $\beta = 4/3$ for a flow with a linear velocity profile and no basal slip. Depth-averaged single-layer models of debris flows and avalanches commonly assume that $\beta = 1$, with little consequent error, but nonuniform velocity distributions can play an important role in momentum exchange that accompanies mass exchange between layers.

[24] An explicit expression for the force per unit area $\Sigma F dz$ in (20) can be obtained in a standard way by considering the driving effect of gravity and resisting effect of Cauchy stresses [e.g., *Malvern*, 1969]. Application of Leibniz' theorem [*Abramowitz and Stegun*, 1964, pp. 11] during depth

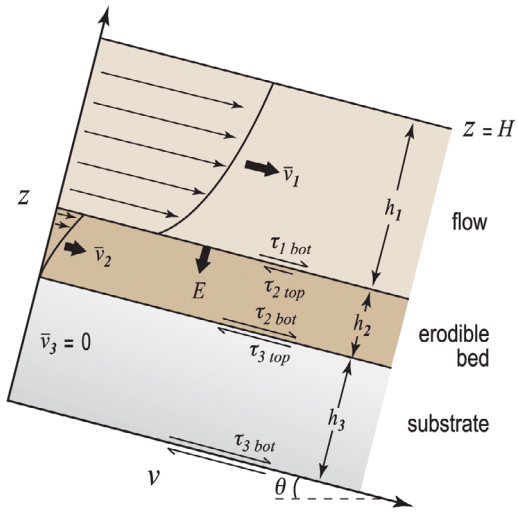

Figure 5. Schematic illustration of velocity profiles $v(z)$, depth-averaged velocities, boundary shear tractions, and thicknesses in a three-layer model of flow interaction with an erodible bed and strong substrate. A velocity and shear-traction discontinuity at the flow-bed boundary influences the downward boundary migration rate (E) due to entrainment of bed sediment.

integration of the resulting stress-gradient terms $\partial\tau_{xx}/\partial x$ and $\partial\tau_{zx}/\partial z$ then yields

$$\int_{z_{bot}}^{z_{top}} \Sigma F dz = \rho g h \sin\theta + \int_{z_{bot}}^{z_{top}} \left[\frac{\partial\tau_{xx}}{\partial x} + \frac{\partial\tau_{zx}}{\partial z}\right] dz$$
$$= \rho g h \sin\theta + \frac{\partial(\bar{\tau}_{xx}h)}{\partial x} - \tau_{xxtop}\frac{\partial z_{top}}{\partial x} + \tau_{xxbot}\frac{\partial z_{bot}}{\partial x} + \tau_{zxtop} - \tau_{zxbot}. \quad (22)$$

In this equation the longitudinal normal stress τ_{xx}, its depth-averaged value $\bar{\tau}_{xx}$, and its boundary values τ_{xxtop} and τ_{xxbot} are reckoned positive in tension, a convention that is necessary in order to establish the correct signs of the boundary shear-traction terms, τ_{zxtop} and τ_{zxbot}. To reconcile this tension-positive sign convention with the compression-positive convention of the normal stress σ_{zz} in (18), I define

$$\sigma_{xx} = -\tau_{xx}, \quad (23)$$

and then use (23) to rewrite (22) as

$$\int_{z_{bot}}^{z_{top}} \Sigma F dz = \rho g h \sin\theta - \frac{\partial(\bar{\sigma}_{xx}h)}{\partial x} + \sigma_{xxtop}\frac{\partial z_{top}}{\partial x} - \sigma_{xxbot}\frac{\partial z_{bot}}{\partial x} + \tau_{zxtop} - \tau_{zxbot}. \quad (24)$$

Taken in order, the six terms on the right-hand side of (24) account for (a) the downslope gravitational driving force, (b) the depth-averaged longitudinal force due to longitudinal thickness and normal-stress gradients, (c) the downslope force due to the compressive longitudinal boundary traction acting on upslope-facing facets of the layer's upper surface, (d) the upslope force due to the compressive longitudinal boundary traction acting on upslope-facing facets of the layer's lower surface, (e) the boundary shear traction acting on the upper surface of a layer, and (f) the boundary shear traction acting on the lower surface of a layer.

[25] Considerable simplification of (24) results from use of an assumption routinely employed in soil and rock mechanics [e.g., *Jaeger*, 1969; *Lambe and Whitman*, 1979],

$$\sigma_{xx} = \sigma_{yy} = \kappa\sigma_{zz}, \quad (25)$$

where κ is a proportionality factor that can play the role of a Rankine earth-pressure coefficient or elastic Poisson's ratio. If the value of κ is constant within any particular layer, as I assume here, then a derivation in Appendix B shows that (24) reduces to

$$\int_{z_{bot}}^{z_{top}} \Sigma F dz = \rho g h \sin\theta - \kappa\rho g h \cos\theta\frac{\partial H}{\partial x} + \tau_{top} - \tau_{bot}, \quad (26)$$

where H is the total thickness of the three-layer system (Figure 5), and the subscript zx has been omitted from τ_{top} and τ_{bot} in order to simplify the notation. Collapse of the three longitudinal stress-gradient terms in (24) into a single term $-\kappa\rho g h \cos\theta(\partial H/\partial x)$ in (26) implies that the effect of $\partial H/\partial x$ is the same in all layers, except insofar as differing layers have differing values of κ and h.

[26] The simplification of (24) that leads to (26) indicates that geometric details of the boundaries between adjacent layers play no role in the theory, but this simplification is contingent on the applicability of (18) and (25). Indeed, these two equations represent the central assumptions that distinguish the elementary theory developed here from a more comprehensive theory that would include the effects of multidimensional, heterogeneous stress fields and thereby resolve the effects of stress variations in the vicinity of boundary irregularities. Such a theory would necessarily involve its own set of constitutive assumptions, however.

[27] Substitution of (26) in (20) yields the x-momentum equation I use to assess the relationship between flow dynamics and entrainment,

$$\rho\left[\frac{\partial(h\bar{v})}{\partial t} + \frac{\partial(\beta h\bar{v}^2)}{\partial x}\right] = \rho g h \sin\theta - \kappa\rho g h \cos\theta\frac{\partial H}{\partial x} + \tau_{top} - \tau_{bot} - \rho v_{top}E_{top} + \rho v_{bot}E_{bot}. \quad (27)$$

Except for the presence of τ_{top} and $\rho v_{top}E_{top}$, (27) has a form like that of a single-layer, depth-averaged flow momentum equation that accounts for possible mass and momentum fluxes through the basal boundary.

[28] A clear relationship between (27) and the slide-block momentum equation (5) can be established if $\beta = 1$, implying that $v(z)$ is constant. For this special case, expansion of the derivatives on the left-hand side of (27) produces some terms that are identical to those on the left-hand side of (19), and use of (19) to cancel these terms introduces a new term, $-\rho\bar{v}E_{top} + \rho\bar{v}E_{bot}$, in (27). Combining this term with the

Table 1. Special Forms of Equation (27) That Apply in Each Layer Illustrated in Figure 5

Layer	Left-Hand Side of (27)	Right-Hand Side of (27)
1 (flow)	$\rho\left[\frac{\partial(h_1\bar{v}_1)}{\partial t}+\frac{\partial(\beta_1 h_1\bar{v}_1{}^2)}{\partial x}\right]$	$\rho g h_1 \sin\theta - \kappa_1\rho g h_1 \cos\theta\frac{\partial H}{\partial x} - \tau_{2top} + \rho v_{2top}E$
2 (erodible bed)	$\rho\left[\frac{\partial(h_2\bar{v}_2)}{\partial t}+\frac{\partial(\beta_2 h_2\bar{v}_2{}^2)}{\partial x}\right]$	$\rho g h_2 \sin\theta - \kappa_2\rho g h_2 \cos\theta\frac{\partial H}{\partial x} + \tau_{1bot} - \tau_{3top} - \rho v_{1\ bot}E$
3 (strong substrate)	0	$\rho g h_3 \sin\theta - \kappa_3\rho g h_3 \cos\theta\frac{\partial H}{\partial x} + \tau_{2bot} - \tau_{3bot}$

boundary momentum-flux terms $-\rho v_{top}E_{top}$ and $+\rho v_{top}E_{top}$ on the right-hand side of (27) then converts (27) to

$$\rho h\frac{d\bar{v}}{dt} = \rho g h\sin\theta - \kappa\rho g h\cos\theta\frac{\partial H}{\partial x} + \tau_{top} - \tau_{bot} + \rho E_{top}(\bar{v} - v_{top}) - \rho E_{bot}(\bar{v} - v_{bot}), \tag{28}$$

where $d/dt = \partial/\partial t + \bar{v}(\partial/\partial x)$ denotes a Lagrangian total time derivative in a frame of reference that translates with the material velocity $\bar{v}$. This Lagrangian form of the momentum equation is correct mathematically but is "non-conservative" physically because its left-hand side describes evolution of $\bar{v}$ rather than the conserved quantity $\rho h\bar{v}$. The importance of this distinction can be clarified by considering a special case in which the upper boundary is a free surface with $\tau_{top} = 0$ and $E_{top} = 0$, and the lower boundary is an eroding surface with $E_{bot} > 0$ and $v_{bot} = 0$. In this case the boundary momentum-flux terms vanish from the Eulerian momentum equation (27), but the Lagrangian equation (28) retains the term $-\rho\bar{v}E_{top}$. The resulting form of (28),

$$\rho h\frac{d\bar{v}}{dt} = \rho g h\sin\theta - \kappa\rho g h\cos\theta\frac{\partial H}{\partial x} - \tau_{bot} - \rho\bar{v}E_{bot}, \tag{29}$$

is closely analogous to the momentum equation used by *McDougall and Hungr* [2005] to analyze the effects of entrainment, and is also closely analogous to the slide-block momentum equation (5). Indeed, except for the term $-\kappa\rho g h\cos\theta(\partial H/\partial x)$, (29) is identical to (5) if τ_{bot} is treated as a Coulomb stress and (5) is divided by the basal area $\Delta x\Delta y$ to find that $m(dv/dt)/(\Delta x\Delta y) = \rho h(dv/dt)$ and $v(dm/dt)/(\Delta x\Delta y) = \rho v E_{bot}$. The close correspondence of (5) and (29) clarifies that, in a Lagrangian reference frame, the term $-\rho\bar{v}E_{bot}$ accounts for the inertia of bed material that is accelerated from rest to reach the ambient flow velocity $\bar{v}$. Use of the term $-\rho\bar{v}E_{bot}$ to evaluate the effects of deposition in a Lagrangian frame is inappropriate, however–for reasons described in conjunction with (5).

[29] No term analogous to $-\rho\bar{v}E_{bot}$ appears in the Eulerian momentum equation (27) because all inertial effects of entrainment or deposition are represented by the left-hand side of (27) unless mass passing through the upper or lower boundaries carries some momentum with it [cf. *Chen et al.*, 2006; *Sovilla et al.*, 2006]. A key advantage of (27) is that it can represent inertial effects more precisely than (28) or (29) can, because it does not require the assumption of a uniform velocity profile (i.e., $\beta = 1$). As shown below, the role of nonuniform velocity profiles is critical when evaluating interactions between adjacent layers.

4.2. Interactions Between Adjacent Layers

[30] Various special forms of (27) apply to the flow, bed, and substrate layers (Table 1). To distinguish these special forms, I use the subscript 1 to designate variables in the overriding flow layer, the subscript 2 for the entrainable bed-sediment layer, and the subscript 3 for the high-strength substrate layer (Figure 5). The equations of Table 1 assume that layer 1 experiences a negligible boundary shear traction on its upper surface. Thus, the only boundary shear traction affecting layer 1 is the resisting shear traction exerted by the top of the underlying sediment bed, $-\tau_{2top}$. The magnitude of $-\tau_{2top}$ may differ from that of the traction the base of the flow exerts on the bed, $+\tau_{1bot}$, owing to a stress-field discontinuity at the flow-bed interface. (Such discontinuities occur commonly in deforming Coulomb materials, for example [*Jaeger*, 1969]). The sediment bed (layer 2) experiences the shear traction $+\tau_{1bot}$ applied at its top surface by the overriding flow and also a resisting basal shear traction applied by the strong substrate, $-\tau_{3top}$. The substrate, in turn, experiences the traction $+\tau_{2bot}$ applied by the overlying bed sediment and the basal resisting traction $-\tau_{3bot}$ at some arbitrarily great depth where $z = 0$ and static stress equilibrium applies.

[31] The only nonzero entrainment rate included in the equations of Table 1 is E at the flow-bed boundary, which is the focus of this analysis. Recall that E is reckoned positive if the boundary migrates downward as mass is transferred from the bed-sediment layer to the flow layer. Thus, if the mass involved in this transfer has nonzero momentum ρv_{2top} per unit volume, the momentum flux into the flow per unit area is $\rho v_{2top}E$, as shown in Table 1. Similarly, if mass is transferred from the flow to the bed during deposition ($E < 0$), the bed layer gains momentum at the rate $-\rho v_{1bot}E$.

[32] The flow and bed layers can exchange momentum only if a velocity contrast exists along their interface, and momentum must be conserved during such an exchange. This requirement has ramifications that can be assessed by first adding the equations for layers 1 and 2 to obtain a momentum-conservation equation for the two-layer system as a whole. The right-hand side of the two-layer equation contains several forcing terms that must cancel one another because $-\tau_{3top}$ accounts for the only external force (aside from gravity) that acts on the two-layer system. This cancellation of terms yields $-\tau_{2top} + \tau_{1bot} + \rho v_{2top}E - \rho v_{1bot}E = 0$, and the two-layer momentum equation thereby reduces to

$$\rho\left[\frac{\partial(h_1\bar{v}_1 + h_2\bar{v}_2)}{\partial t} + \frac{\partial(\beta_1 h_1\bar{v}_1{}^2 + \beta_2 h_2\bar{v}_2{}^2)}{\partial x}\right] = (h_1 + h_2)\rho g\sin\theta - (h_1\kappa_1 + h_2\kappa_2)\rho g\cos\theta\frac{\partial H}{\partial x} - \tau_{3top}. \tag{30}$$

The terms canceled from (30) can be rearranged to obtain

$$\left[\tau_{1bot} - \tau_{2top}\right] + \rho E\left[v_{2top} - v_{1bot}\right] = 0. \tag{31}$$

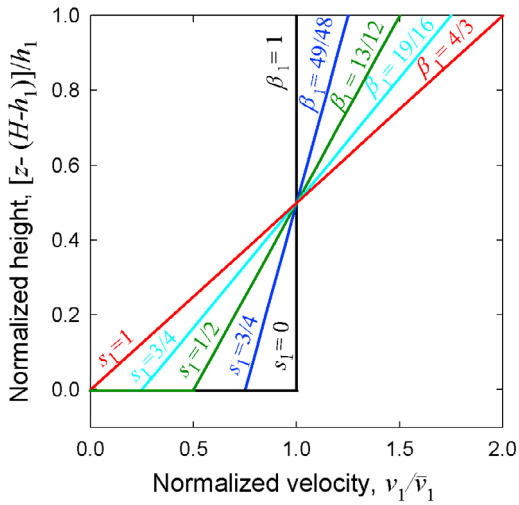

Figure 6. Graphs of equation (33), illustrating some alternative flow velocity profiles, $v_1(z)$. The parameter s_1 specifies the fraction of downslope motion accommodated by simple shear deformation as opposed to basal slip. The parameter β_1 is the corresponding momentum distribution coefficient.

Importantly, the expressions in brackets in (31) can describe jumps (i.e., finite changes) in shear tractions and velocities that may exist at the flow-bed interface. If such jumps do not exist, then there is little reason to treat layers 1 and 2 as mechanically distinct, and equation (30) contains all the pertinent depth-integrated information about momentum conservation in the two-layer system. If jumps do exist, however, then equation (31) contains crucial information that supplements the flow- and bed-layer equations of Table 1.

[33] A result similar to (31) has been obtained previously by applying general Rankine-Hugoniot jump relationships to bed-erosion problems [*Fraccarollo and Capart*, 2002], but here (31) is derived directly from depth-integrated conservation laws. In the present context (31) is the only relevant jump condition, because the normal-stress distribution described by (18) is continuous across the boundary, and the mass distribution is continuous across the boundary by virtue of the constant bulk density ρ assumed for the flow and bed material [cf. *Chadwick*, 1976, pp. 114–120].

5. Entrainment-Rate Equations and Predictions

[34] Rearrangement of (31) shows that momentum conservation demands that the bed-sediment entrainment rate obeys

$$E = \frac{\tau_{1bot} - \tau_{2top}}{\rho(v_{1bot} - v_{2top})}. \tag{32}$$

The numerator of this equation can be interpreted as an excess boundary shear stress, which expresses the difference between the basal shear traction exerted by the flow (τ_{1bot}) and the boundary shear resistance exerted by the bed (τ_{2top}). The proportionality of E to $\tau_{1bot} - \tau_{2top}$ is consistent with some longstanding ideas about threshold conditions for entrainment of bed sediment [e.g., *Vanoni*, 1975]. On the other hand, the denominator of (32) indicates that E decreases as the basal slip velocity v_{1bot} increases – a result that contradicts conventional wisdom but corroborates the results of the slide-block analysis in section 3.

[35] Two other implications of (32) warrant mention. First, the numerator of (32) implies that deposition rather than entrainment occurs if $\tau_{1bot} < \tau_{2top}$, provided that $v_{1bot} > v_{2top}$. Second, the denominator of (32) indicates that $E \to \infty$ if $\tau_{1bot} > \tau_{2top}$ and $v_{1bot} = v_{2top}$, consistent with the view that layers 1 and 2 behave as a single layer if there is no velocity contrast at the flow-bed interface. The condition $E \to \infty$ implies that downslope motion of the bed occurs en masse in response to quasistatic forcing, as envisaged by *Takahashi* [1978]. Indeed, this is the only style of bed motion that is feasible in the absence of basal boundary slip that transfers downslope flow momentum to the bed. In this case τ_{2top} instantaneously jumps to τ_{3top} as bed acceleration penetrates to a horizon at $z = H - (h_1 + h_2)$, where a stronger substrate prevents motion. The remainder of this section emphasizes scenarios in which motion of the bed is localized at the flow-bed interface and E remains finite, but the next section revisits the possibility of deeper bed deformation.

[36] To further utilize (32) in assessments of finite entrainment rates, it is helpful to relate v_{1bot} to a more readily observed quantity such as $\bar{v}_1$. The relationship between v_{1bot} and $\bar{v}_1$ depends on the flow velocity profile, $v_1(z)$, but for flows of opaque geological debris, direct measurements of $v_1(z)$ are at best problematic–and are perhaps impossible. Distinctions between alternative velocity profiles that involve various combinations of homogeneous simple shear and basal slip have been made on the basis of particle tracking studies, however [*Johnson et al.*, 2012]. This family of profiles can be represented mathematically by

$$\frac{v_1}{\bar{v}_1} = 1 - s_1 + 2s_1 \frac{z - (H - h_1)}{h_1}, \tag{33}$$

where s_1 is a fitting parameter that ranges from $s_1 = 0$ if there is no simple shear to $s_1 = 1$ if there is no basal slip (Figure 6). Equation (33) implies that $v_{1bot} = (1 - s_1)\bar{v}_1$. As a result, for a broad range of plausible velocity profiles, (32) can be expressed as

$$E = \frac{\tau_{1bot} - \tau_{2top}}{\rho[(1 - s_1)\bar{v}_1 - v_{2top}]}. \tag{34}$$

Johnson et al. [2012] showed that for large-scale experimental debris flows, a good fit to particle-tracking data was attained with $s_1 = 1/2$, implying that the basal slip velocity was half the mean flow velocity. The momentum distribution coefficient defined by (21) can also be expressed in terms of s_1,

$$\beta_1 = 1 + (1/3)s_1^2, \tag{35}$$

indicating that $s_1 = 1/2$ corresponds to $\beta_1 = 13/12$ (Figure 6). Thus, the entrainment-rate predictions of (34) can be very sensitive to small deviations of β_1 from unity.

[37] An important special form of (34) applies for boundary conditions analogous to those considered in the slide-block model of section 3. In such cases the top of the

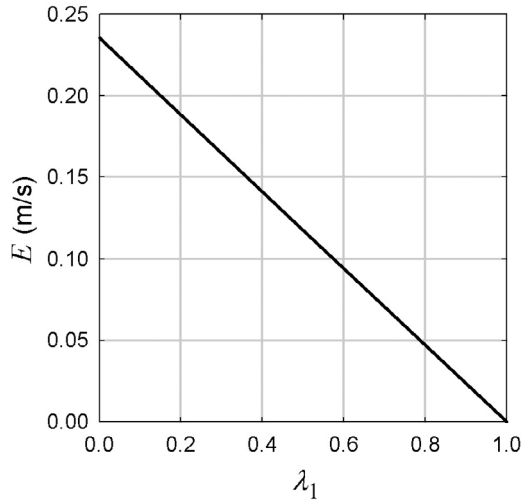

Figure 7. Graph of equation (41), illustrating entrainment rates, E, predicted as a function of the degree of flow liquefaction, λ_1, if other parameters are assigned values commensurate with those in the debris-flow entrainment experiments of *Iverson et al.* [2011] and *Reid et al.* [2011]: $\mu_1 = 0.84$, $g = 9.8$ m/s^2, $h_1 \approx 0.2$ m, $\theta = 31°$, and $\bar{v}_1 \approx 12$ m/s.

bed-sediment layer is static prior to entrainment, and the boundary shear tractions τ_{1bot} and τ_{2top} each obey a Coulomb friction rule $\tau = \mu\sigma'_{zz}$ that incorporates a standard definition of effective normal stress,

$$\sigma'_{zz} = \sigma_{zz} - p, \tag{36}$$

where p is pore fluid pressure. Provided that the total normal stress σ_{zz} satisfies (18), boundary shear tractions that satisfy $\tau = \mu\sigma'_{zz}$ can be expressed as

$$\tau_{1bot} = \mu_1(\sigma_{zz\,1bot} - p_{1bot}) = \mu_1(\rho g h_1 \cos\theta - p_{1bot}), \tag{37}$$

$$\tau_{2top} = \mu_2(\sigma_{zz\,2top} - p_{2top}) = \mu_2(\rho g h_1 \cos\theta - p_{2top}), \tag{38}$$

where μ_1 and μ_2 are Coulomb friction coefficients for layers 1 and 2, respectively, and p_{1bot} and p_{2top} are boundary pore fluid pressures for layers 1 and 2. By incorporating (37) and (38), (34) becomes

$$E = \frac{\rho g h_1(\mu_1 - \mu_2)\cos\theta + \mu_2 p_{2\,top} - \mu_1 p_{1\,bot}}{(1 - s_1)\rho\bar{v}_1}. \tag{39}$$

This equation indicates that $E > 0$ requires a contrast in Coulomb friction coefficients ($\mu_1 > \mu_2$), a contrast in pore fluid pressures ($p_{2top} > p_{1bot}$), or some combination of the two.

[38] A contrast that leads to $E > 0$ in (39) can result from rate-dependent friction that causes $\mu_1 > \mu_2$ to arise from shearing of basal flow material, analogous to the behavior represented in equation (4). Although no experiments have been conducted to isolate this effect in realistic debris-flow materials, recent ring-shear experiments with concentrated mixtures of solid spheres and liquid show that rate-dependent friction becomes significant if the value of a key dimensionless parameter, I_v, exceeds about 10^{-4} [*Boyer et al.*, 2011]. Re-expressed here using the notation

$$I_v = \frac{\eta\dot{\gamma}_1}{\sigma'_{zz\,1bot}}, \tag{40}$$

this parameter includes the pore fluid viscosity η (which has values ranging from about 10^{-2} to 10^{-1} Pa-s in many debris-flow mixtures), and the bulk shear rate $\dot{\gamma}_1$ (which probably has values exceeding 10 s^{-1} at the base of many rapid debris flows) [*Iverson*, 1997]. These values imply that $I_v > 10^{-4}$ may commonly apply in flows with basal effective normal stresses that satisfy $\sigma'_{zz1bot} \leq 1$ kPa . Partial debris-flow liquefaction can produce basal effective normal stresses this small [*Iverson et al.*, 2010], providing the requisite conditions to produce $\mu_1 > \mu_2$ in (39).

[39] Contrasts in boundary pore fluid pressure also can promote entrainment. For example, if the top of the bed sediment becomes completely liquefied by high pore pressures (i.e., $p_{2top} = \rho g h_1 \cos\theta$) and the value $s_1 = 1/2$ is adopted to describe the flow velocity profile, then (39) reduces to

$$E = \frac{2\mu_1 g h_1 \cos\theta(1 - \lambda_1)}{\bar{v}_1}, \tag{41}$$

where

$$\lambda_1 = p_{1bot}/\rho g h_1 \cos\theta \tag{42}$$

is a pore pressure ratio that indicates the degree of flow liquefaction ($0 \leq \lambda_1 \leq 1$) [cf. *Iverson and Denlinger*, 2001]. Strength reduction due to growth of pore pressure in overridden bed sediment also has implications for evolution of flow momentum. The flow momentum equation of Table 1 contains only one resistance term, $-\tau_{2top}$, which describes the shear traction exerted by the underlying bed sediment. With a nearly liquefied Coulomb bed ($\tau_{2top} \approx 0$), there is little resistance to flow acceleration other than the inertial reaction force that develops during entrainment of bed sediment. Thus, the mass and momentum of a flow that liquefies its bed can grow explosively [*Iverson et al.*, 2011].

[40] Predictions of (41) can be compared with entrainment rates of 0.05 to 0.1 m/s measured in large-scale experiments in which wet sediment beds liquefied almost completely as they were overridden by debris flows [*Iverson et al.*, 2011; *Reid et al.*, 2011]. Applicable parameter values in these experiments were $\mu_1 = 0.84$, $g = 9.8$ m/s^2, $h_1 \approx 0.2$ m, $\theta = 31°$, and $\bar{v}_1 \approx 12$ m/s, and use of these values in (41) yields a graph of E predicted as a function of λ_1 (Figure 7). The graph shows that entrainment rates in the observed range of 0.05 to 0.1 m/s result if λ_1 values range from about 0.5 to 0.8, consistent with λ_1 values typically measured in experimental debris flows [*Iverson et al.*, 2010]. Furthermore, Figure 7 shows that the full range of plausible entrainment rates extends upward only to ~0.23 m/s for the conditions in the experiments. This upper bound on sustainable entrainment rates results from constraints imposed by momentum conservation with $\bar{v}_1 = 12$ m/s.

[41] Predictions of (41) also can be compared with entrainment-rate measurements at the Chalk Cliffs field site in Colorado [*Coe et al.*, 2008; *McCoy et al.*, 2010]. There, relevant parameter values when debris flows overrode wet bed sediment at the upper monitoring station on June 12,

2010 were $\mu_1 = 0.97$, $h_1 \approx 0.88$ m, $\theta = 13°$, and $\bar{v}_1 \approx 3.9$ m/s (McCoy et al., submitted manuscript, 2012). Use of these values in (41) yields entrainment rates ranging from $E = 0$ for $\lambda_1 = 1$ to $E = 4.2$ m/s for $\lambda_1 = 0$. Independent constraints on λ_1 did not exist for this Chalk Cliffs event, but adoption of typical debris-flow values $0.5 \le \lambda_1 \le 0.8$ leads to predicted E values an order of magnitude larger than the measured values of 0.14 m/s. This discrepancy is consistent with the fact that full bed liquefaction did not occur at the Chalk Cliffs site (McCoy et al., submitted manuscript, 2012). Under such conditions, (39) may be a more-appropriate entrainment-rate equation than (41), but (39) includes additional quantities unconstrained by measurements at Chalk Cliffs.

[42] Further understanding of entrainment predictions can be gained by establishing a precise relationship between equation (39) and the slide-block entrainment-rate equation (13). Making the substitutions $m = \rho h_1 \Delta x \Delta y$, $dm/dt = \rho E \Delta x \Delta y$, and $\mu_0 = \mu_2$ in (13) converts it to the equivalent continuum-mechanical form

$$E = \frac{\alpha G h}{v} = \alpha \frac{\rho g h_1 \sin\theta - \mu_2 \rho g h_1 \cos\theta}{\rho v}. \tag{43}$$

After setting $s_1 = 0$ and $v = \bar{v}_1$ in (39) to mimic block-style motion, equation (39) matches (43) if the entrainment-efficiency parameter α is defined as

$$\alpha = \frac{\rho g h_1 (\mu_1 - \mu_2)\cos\theta - (\mu_1 p_{1\,bot} - \mu_2 p_{2top})}{\rho g h_1 \sin\theta - \mu_2 \rho g h_1 \cos\theta}. \tag{44}$$

Equation (44) demonstrates that α depends on the ratio of the excess boundary shear traction $\rho g h_1(\mu_1 - \mu_2)\cos\theta - (\mu_1 p_{1bot} - \mu_2 p_{2top})$ to the net driving force per unit area at the base of the slide block, $\rho g h_1 \sin\theta - \mu_2 \rho g h_1 \cos\theta$. At steady state (i.e., with no slide-block acceleration) these two quantities are equal, such that $\alpha = 1$ and the slide-block mass grows at the maximum sustainable rate indicated by (14)–(17).

[43] The same interpretation of the numerator and denominator of (44) applies if pore pressure effects are absent, in which case (44) reduces to the simple form,

$$\alpha = \frac{\mu_1 - \mu_2}{\tan\theta - \mu_2}. \tag{45}$$

This equation demonstrates that the relationship $\tan\theta \ge \mu_1 \ge \mu_2$ must be satisfied to ensure that $0 \le \alpha \le 1$. Thus, as stated in section 3, the slide-block model implies that sustained entrainment of dry, cohesionless Coulomb material can occur only if the bed slopes steeply enough to fail under static gravitational loading. On lesser slopes, entrainment can be a transient process accompanied by flow deceleration (as observed by *Mangeney et al.* [2010]), or it can result from transient growth of pore fluid pressure that weakens bed sediment as it is overridden.

6. Bed Deformation and Pore Pressure Generation

[44] The potential for bed deformation that leads to pore pressure growth depends partly on the weight of the overriding flow but also on downslope momentum transferred to the bed by the flow. The effects of this transfer are evident in the bed-layer momentum equation of Table 1, and are clearest if longitudinal gradients are neglected in the equation (i.e., $\partial/\partial x = 0$), reducing it to

$$\rho \frac{\partial(h_2 \bar{v}_2)}{\partial t} = \rho g h_2 \sin\theta + \tau_{1bot} - \tau_{3top} - \rho v_{1bot} E. \tag{46}$$

In this case the kinematic boundary condition (A5) of Appendix A reduces to $E = -\partial h_2/\partial t$, and use of this relationship permits $\partial(h_2\bar{v}_2)/\partial t = h_2 \partial\bar{v}_2/\partial t - \bar{v}_2 E$ to be substituted into (46). The resulting bed momentum equation can then be rearranged to obtain

$$\rho[E(v_{1bot} - \bar{v}_2) + h_2(\partial\bar{v}_2/\partial t)] = \tau_{1bot} - \tau_{3top} + \rho g h_2 \sin\theta. \tag{47}$$

Consistent with (32), (47) reduces to $E = [\tau_{1bot} - \tau_{2top}]/\rho v_{1bot}$ if the bed material is entirely static, because the values $\bar{v}_2 = 0$ and $\tau_{3top} = \tau_{2top} + \rho g h_2 \sin\theta$ then apply. Otherwise, (47) indicates that the net external force per unit area acting on the bed layer, $\tau_{1bot} - \tau_{3top} + \rho g h_2 \sin\theta$, may accelerate the layer at the depth-averaged rate $\partial\bar{v}_2/\partial t$ and also confer the velocity v_{1bot} to boundary material entrained by the overriding flow at rate E. Both phenomena can occur simultaneously, but (47) shows that increased values of $\partial\bar{v}_2/\partial t$ imply diminished values of E, and vice versa. In the limit $h_2 \to 0$, (47) reduces to the jump condition (31) because the identities $\tau_{3top} \equiv \tau_{2top}$ and $\bar{v}_2 \equiv v_{2top}$ apply. In this case entrainment and bed-layer acceleration are indistinguishable.

[45] The details of bed deformation that may occur prior to entrainment cannot be resolved by a depth-integrated analysis, but the potential for pore pressure growth during bed deformation can be assessed by utilizing a constitutive equation that specifies how changes in porosity, n, are related to shear deformation and changes in the mean effective normal stress, $\bar{\sigma}'$ [cf. *Iverson*, 2009; *George and Iverson*, 2011]:

$$\frac{1}{1-n}\frac{dn}{dt} = \dot{\gamma}_2 \tan\psi - C\frac{d\bar{\sigma}'}{dt}. \tag{48}$$

Here $\dot{\gamma}_2$ is the bed-sediment shear rate associated with $\bar{v}_2 > 0$, ψ is a dilatancy angle that describes the tendency of the sediment to dilate ($\psi > 0$) or contract ($\psi < 0$) during irreversible shearing, C is the drained compressibility of the sediment-fluid mixture (here assumed to greatly exceed the compressibility of the solid and fluid constituents), and d/dt is a total time derivative in a frame of reference that moves with the deforming sediment. If shearing were to occur in a closed container that prevents volume change, then (48) would reduce to $d\bar{\sigma}'/dt = \dot{\gamma}_2 \tan\psi/C$, implying that $\bar{\sigma}'$ would increase with time if shearing proceeded with $\psi > 0$. This specious prediction demonstrates that ψ cannot be a material constant. Rather, ψ must evolve and must become zero during steady state shearing with no volume change – a state known in soil mechanics as a critical state [*Schofield and Wroth*, 1968]. With $\psi = 0$ or $\dot{\gamma}_2 = 0$, (48) reduces to the standard constitutive equation used to define compressibility in soil consolidation theories, $C = -[1/(1-n)](dn/d\bar{\sigma}')$ [*Bear*, 1972, pp. 206], and with $C = 0$ or $d\bar{\sigma}'/dt = 0$, (48) reduces to a kinematic description of porosity change due to diltatant shearing.

[46] Changes in porosity described by (48) imply corresponding changes in ρ, because $\rho = \rho_f n + \rho_s(1-n)$, where ρ_f

and ρ_s are the mass densities of the fluid and solid constituents of the bed sediment. For water-saturated sediment with realistic ranges of ρ_f, ρ_s, and n values, however, implied changes in ρ are less than about 10 percent. Thus, use of a constant ρ is unlikely to produce significant errors in order-of-magnitude assessments of pore pressure responses. Use of a constant ρ also enables the mean effective normal stress in (48) to be defined more explicitly. By combining (18), (25), and (36), $\bar{\sigma}'$ can be expressed as

$$\bar{\sigma}' = \frac{\sigma_{xx} + \sigma_{yy} + \sigma_{zz}}{3} - p = \frac{1 + 2\kappa_2}{3}\rho g(H - z)\cos\theta - p. \quad (49)$$

An unambiguous relationship between the porosity change described by (48) and attendant pore pressure evolution can be obtained if the sediment bed behaves as effectively water-saturated. Experimental evidence indicates that such behavior does not require complete saturation, but also indicates that distinctly different behavior occurs when beds are relatively dry [*Iverson et al.*, 2011; *Reid et al.*, 2011]. For a saturated bed, mass-conservation equations for the bed's solid and fluid constituents may be combined with Darcy's law for pore fluid flow to obtain

$$\frac{1}{1-n}\frac{dn}{dt} = \frac{k}{\eta}\nabla^2 p, \quad (50)$$

where k is the Darcian permeability, and η is the pore fluid viscosity. A generalized form of (50) accounts for the effects of variations in k and η [*Iverson*, 2005], but here both parameters are treated as constants in order to highlight essential aspects of pore pressure evolution.

[47] Combination of (48), (49) and (50) yields a pore pressure diffusion equation,

$$\frac{dp}{dt} = \frac{k}{C\eta}\nabla^2 p + \frac{1 + 2\kappa_2}{3}\rho g\cos\theta\frac{d(H - z)}{dt} - \frac{\dot{\gamma}_2\tan\psi}{C}, \quad (51)$$

which shows how evolution of p in a Lagrangian frame of reference depends on the diffusivity $k/C\eta$ and on two types of forcing. One type of forcing arises from increases in flow surface height H or from downward motion of the Lagrangian z coordinate ($d(H - z)/dt > 0$), both of which lead to gravity-driven pressurization of the pore fluid. The other type of forcing involves pore pressure modification due to shear-induced bed dilation at the rate $\dot{\gamma}_2\tan\psi$. If $\psi > 0$, then pore pressure tends to decline as a consequence of shearing, whereas pore pressure tends to increase if $\psi < 0$.

[48] In the limiting case with $k/C\eta \to 0$, equation (51) reduces to a description of undrained bed behavior. In this case p changes instantaneously and uniformly in response to compressional loading or shearing that causes pore-volume change. *Hutchinson and Bhandari* [1971] first highlighted the role of undrained compression that may occur when mass movements override water-laden sediment, and *Sassa* [1985] extended the concept to include undrained shearing of sediments beneath debris flows. Pore pressure responses during undrained deformation can be muted by the influence of the compressibilities of the individual solid and fluid constituents [*Skempton*, 1954; *Rice and Cleary*, 1976], but this influence is generally negligible in water-saturated, soil-like materials at low confining stresses typical of Earth's surface [*Lade and De Boer*, 1997].

[49] If $k/C\eta \to 0$ does not apply, then the deforming bed layer behaves as variably drained, and the effects of compression and shearing on p depend on their rates relative to the rate of diffusive dissipation of pore pressure [cf. *Rudnicki*, 1984; *Iverson and LaHusen*, 1989; *Iverson et al.*, 1997]. The magnitude of these rate effects can be quantified by identifying the diffusion timescale as $T = C\eta h_2^2/k$ and the pressure scale as $P = \rho g h_2\cos\theta$, and then multiplying all terms of (51) by T/P to obtain a normalized equation

$$\frac{dp^*}{dt^*} = \nabla^{2*}p^* + \frac{1 + 2\kappa_2}{3}\frac{d(H^* - z^*)}{dt^*} - I_2\frac{\tan\psi}{\cos\theta}. \quad (52)$$

Here $p^* = p/P$, $t^* = t/T$, $\nabla^{2*} = \nabla^2 h_2^2$, $H^* = H/h_2$, $z^* = z/h_2$, and $I_2 = \dot{\gamma}_2 T/CP$ is a dimensionless parameter that involves the timescale ratio $\dot{\gamma}_2 T$ and normalized characteristic pressure CP.

[50] Equation (52) indicates that the compression effects expressed by $d(H^* - z^*)/dt^* > 0$ are of the same order as the diffusion effects expressed by $\nabla^{2*}p^*$, whereas the magnitude of shearing effects depends on the value of I_2. Algebraic substitutions show that this parameter can be defined in terms of its primitive components as

$$I_2 \equiv \frac{h_2\dot{\gamma}_2\eta}{k\rho g}. \quad (53)$$

Values of some of the components of I_2 are readily estimated for water-saturated sediment beds ($\eta \approx 10^{-3}$ Pa-s, $\rho \approx 2000$ kg/m^3, $g \approx 9.8$ m/s^2), and use of these values and a uniform simple-shear approximation $\dot{\gamma}_2 \approx 2\,\bar{v}_2/h_2$ in (53) reduces the expression for I_2 to

$$I_2 \approx (10^{-7}\text{m-s})\frac{\bar{v}_2}{k}. \quad (54)$$

Because values of k can range widely, from about 10^{-7} m^2 for gravel to 10^{-17} m^2 for silty clay [*Freeze and Cherry*, 1979], (54) implies that the value of I_2 can also range widely.

[51] A graph of (54) indicates that if sand or finer sediment is present in a bed that is overridden by a debris flow or avalanche, slight shear displacements of the bed can play a dominant role in generating pore fluid pressure. Indeed, with sufficient fine sediment, $I_2 \gg 1$ applies even for depth-averaged displacement rates as small as $\bar{v}_2 = 10^{-6}$ m/s (Figure 8). In this case behavior is effectively undrained. Pore pressure generation can then produce very strong feedback (either positive or negative, depending on the sign of ψ) that influences further bed deformation and acceleration of the overriding flow. By contrast, shearing of beds composed entirely of sediment that is gravel-sized or coarser is likely to satisfy $I_2 \ll 1$ (Figure 8). In this case shear deformation is almost perfectly drained and is apt to generate little pore fluid pressure. Of course, if $I_2 \approx 1$, then intermediate responses that are not well-characterized as either drained or undrained are possible.

[52] Contractive shear displacements probably played an important role in causing liquefaction and rapid entrainment of wet bed sediment and explosive growth of debris-flow momentum in the experiments of *Iverson et al.* [2011] and *Reid et al.* [2011]. In these experiments loosely packed sediment beds consisting of gravel and loamy sand had k values in the range from 4×10^{-11} to 4×10^{-12} m^2 [*Iverson et al.*, 2010]. According to Figure 8, these values imply that depth-

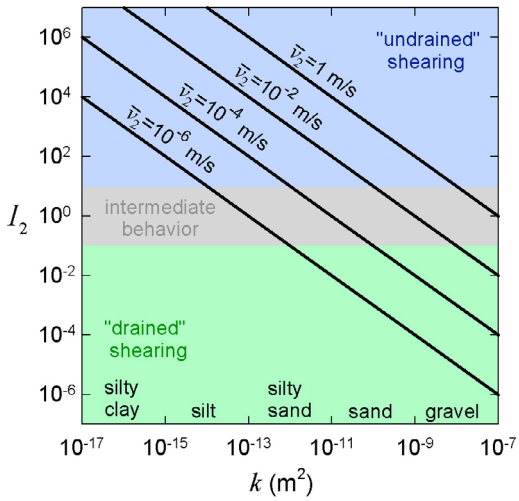

Figure 8. Graphs of equation (54), illustrating variation of the parameter I_2 as a function of hydraulic permeability k for a range of depth-averaged bed displacement rates, $\bar{v}_2$. Labels along the horizontal axis identify textures of sediments that typically exhibit the adjacent k values (adapted from *Freeze and Cherry* [1979]). Shaded regions identify ranges of I_2 values indicative of shear behavior that can be characterized as "drained," "undrained," or "intermediate."

averaged bed displacement rates of roughly 10^{-3} m/s sufficed to produce $I_2 \geq 10$.

7. Discussion

[53] The preceding analyses show that, if all other factors are equal, conservation of downslope momentum demands that bed sediment entrainment rates decline as basal flow velocities increase. Although conventional wisdom holds that increasing a flow's velocity generally enhances its capacity for sediment entrainment, much of this wisdom derives from experience with near-equilibrium fluvial systems. Understanding of these systems has a context that differs fundamentally from that considered here, because it typically focuses on flows with macroscopic momentum that does not respond to entrainment, rather than on flows with fully coupled evolution of flow and bed momentum. The sharp contrast between fixed-momentum and evolving-momentum perspectives makes it worthwhile to recapitulate the prediction $E \sim 1/v_{1bot}$ by using an analogy that appeals to kinesthetic intuition. In this analogy a human plays the role of a moving flow with evolving momentum.

[54] Consider a man descending a long version of a children's playground slide with a constant slope and constant friction coefficient. If the man is unencumbered as he descends, he has a constant acceleration and a basal slip velocity, v_{1bot}, that increases linearly with time. However, the man is tasked with entraining static bricks that are positioned alongside the slide. Each brick has the same fixed mass and volume. Therefore, the entrainment rate is the local volumetric rate (per unit basal area) at which the man acquires bricks and accelerates them to his speed. The man's momentum is unaffected by his entrainment of static bricks, which have no momentum to contribute, but momentum conservation dictates that his downslope acceleration decreases in response to the force he exerts to perform the entrainment.

[55] Next consider an ideal case in which the man and the bricks are perfectly lubricated. Assume that the man has assistants (who may also be lubricated) positioned adjacent to the slide. The assistants push bricks laterally onto the man's lap as he passes by, allowing him to acquire bricks without exerting force or doing work. Nevertheless, to complete the task of entrainment, the man must exert a force to accelerate each brick and bring it up to his speed, counteracting the force that each brick exerts on him. The time integral of this force (i.e., the impulse) equals the mass of the brick multiplied by v_{1bot}, which is the change in the brick's velocity as it comes up to speed. The man's downslope acceleration, integrated over the duration of the impulse, decreases in proportion to the magnitude of the impulse, and if the brick's mass or the man's speed is large enough, the impulse may produce a net negative acceleration that slows the man down. Whether or not slowing occurs, there is a tradeoff between the man's speed and the impulsive force he must exert to accelerate each brick, and this tradeoff dictates that $E \propto 1/v_{1bot}$. The tradeoff is a purely inertial phenomenon that is independent of the work done by the man to acquire bricks.

[56] In more-complicated circumstances the man or the bricks may be imperfectly lubricated, or his assistants may be absent, requiring the man to do additional work to pick up bricks before accelerating them. The added force required to do this work can be characterized, albeit imprecisely, as friction. The effects of friction are analogous to those of incomplete liquefaction of bed sediments, and they reduce the man's maximum rate of brick entrainment if all other factors remain unchanged. A further complication exists if the man is able to reduce his basal friction as he slides, analogous to a debris flow or avalanche that can liquefy its bed as it overrides it. Reduction of basal friction is the only means by which the momentum of the man or an analogous flow can grow more rapidly than it would in the absence of entrainment. In such circumstances flow momentum can grow unstably, however, because the net force available to cause entrainment grows in proportion to the mass of the entraining body [e.g., *Iverson et al.*, 2011].

8. Caveats

[57] Although elementary mechanics establishes some important relationships between momentum conservation and bed-sediment entrainment, additional details remain unresolved, and some cannot be assessed using a depth-integrated continuum model. Like many geomechanical models, the depth-integrated continuum model presented here assumes that bed-normal total stresses (σ_{zz}) are lithostatic and that longitudinal normal stresses are proportional to σ_{zz}. These assumptions lead to useful mathematical simplifications and physical inferences, but they preclude assessment of the effects of boundary irregularities–except insofar as these effects can be parameterized by a boundary friction coefficient. If elements of bed material protrude a significant distance into an overriding flow, for example, shear tractions along the boundary vary spatially. Furthermore, as the flow impinges against such protuberances, it can transfer x-momentum to the bed by a mechanism that involves

not only variable shear tractions but also variable normal tractions–an effect commonly parameterized as form drag. An inability to assess these effects of boundary geometry represents a fundamental limitation of the depth-averaged entrainment model presented here.

[58] From a practical viewpoint, perhaps a more significant limitation results from the model's focus on bed-sediment entrainment and neglect of entrainment of bank material. Rigorous modeling of bank entrainment, while very desirable, would be very challenging. It would entail formulation of a multidimensional boundary-traction model (in which depth averaging would likely be inappropriate), and would also entail coupling the traction model with a three-dimensional bank-failure model (because bank failures with infinite lengths or widths would contribute infinite mass to a passing flow). Moreover, a model of bank-material entrainment by debris flows or avalanches would necessarily include fully coupled evolution of flow momentum, distinguishing it from models of morphological evolution of stream banks that occurs under macroscopically steady flow conditions.

9. Conclusions

[59] Conservation of momentum constrains interpretations and predictions of bed-sediment entrainment rates by debris flows and avalanches that are free to accelerate as they descend steep slopes. Both a Coulomb slide-block analysis and a depth-integrated continuum analysis predict that, if all other factors are constant, the entrainment rate E decreases as the basal flow velocity v_{1bot} increases. The largest sustainable entrainment rates occur in conjunction with steady flow, because the entire net driving force is then allocated to entrainment rather than acceleration. These findings help explain some key results of entrainment experiments in which dry granular avalanches moved across sloping beds covered with the same material [*Mangeney et al.*, 2010]: entrainment was more pronounced during relatively slow, steady motion of avalanches than during rapidly accelerating motion.

[60] Predicted entrainment rates depend not only on flow velocities but also on excess boundary shear tractions. Although no universal model of shear tractions exists, a Coulomb model accounts for the effects of friction as well as modifications of bed friction due to pore fluid pressure. Entrainment-rate predictions are simplest if pore pressures in bed sediment locally grow large enough to liquefy it when it is overridden. Then the resisting Coulomb shear traction is essentially zero, and entrainment can occur at the maximum sustainable rate, expressed by $E = [\mu_1 g h_1 \cos\theta(1-\lambda_1)]/v_{1bot}$ or by $E = [2\mu_1 g h_1 \cos\theta(1-\lambda_1)]/\bar{v}_1$ if the approximation $v_{1bot} \approx \bar{v}_1/2$ is adopted. The latter equation predicts entrainment rates similar to those measured in large-scale debris-flow experiments in which wet bed sediments liquefied almost completely when they were overridden [*Iverson et al.*, 2011; *Reid et al.*, 2011].

[61] Growth of pore fluid pressure in wet bed sediment can occur as a result of both compressional loading by an overriding flow and shear deformation of the bed in response to transfer of downslope flow momentum. Loosely packed beds that exhibit contractive shear behavior are especially susceptible to this type of pore pressure growth, which may lead to liquefaction. An analysis of pore pressure generation and diffusion shows that the propensity for liquefaction may be very large, for example, if a water-saturated bed that contains significant sand or finer sediment begins to creep downslope at a depth-averaged rate greater than about 10^{-3} m/s as it is overridden. Bed liquefaction also promotes flow momentum growth, because it minimizes basal resisting forces that impede downslope acceleration.

[62] Evolution of flow momentum during entrainment illustrates a fundamental asymmetry in the relationships governing growth of mass, velocity and momentum for Coulomb bodies. Whereas a Coulomb body of constant mass undergoes stable velocity growth while descending a steeply inclined plane, a Coulomb body with constant velocity can undergo exponential mass growth in the same circumstances – provided that the frictional resistance of the bed is low enough to allow entrainment. This unbounded mass growth in turn implies unstable momentum growth. Therefore, the maximum momentum attainable by Coulomb bodies that entrain basal material is limited only by the volume of steeply sloping, erodible material they encounter.

Appendix A: Depth Integration of Conservation Equations

[63] The general differential equations describing conservation of mass and the x component of momentum in a continuous material with variable bulk density ρ can be written as

$$\frac{\partial\rho}{\partial t} + \frac{\partial(\rho v_x)}{\partial x} + \frac{\partial(\rho v_y)}{\partial y} + \frac{\partial(\rho v_z)}{\partial z} = 0, \tag{A1}$$

$$\begin{aligned}\frac{\partial(\rho v_x)}{\partial t} + \frac{\partial(\rho v_x^2)}{\partial x} + \frac{\partial(\rho v_x v_y)}{\partial y} + \frac{\partial(\rho v_x v_z)}{\partial z} &= \rho g_x + \frac{\partial\tau_{xx}}{\partial x} + \frac{\partial\tau_{yx}}{\partial y} + \frac{\partial\tau_{zx}}{\partial z} \\ &= \Sigma F_x. \end{aligned} \tag{A2}$$

where v_x, v_y, and v_z, are, respectively, the x, y, and z components of velocity, ρg_x is the driving force per unit volume due to the x component of the material's weight, and τ_{xx}, τ_{yx} and τ_{zx} are the components of the Cauchy stress tensor that resist motion in the x direction. For a discrete layer of material, depth averages of the dependent variables in (A1) and (A2) are defined as

$$\begin{aligned}\bar{\rho}(x,y,t) &= \frac{1}{h}\int_{z_{bot}}^{z_{top}} \rho dz \quad \bar{v}_x(x,y,t) = \frac{1}{h}\int_{z_{bot}}^{z_{top}} v_x dz, \\ \bar{v}_y(x,y,t) &= \frac{1}{h}\int_{z_{bot}}^{z_{top}} v_y dz \quad \bar{v}_z(x,y,t) = \frac{1}{h}\int_{z_{bot}}^{z_{top}} v_z dz,\end{aligned} \tag{A3}$$

where $z_{bot}(x, y, t)$ is the z coordinate of the layer's basal surface, $z_{top}(x, y, t)$ is the z coordinate of the layer's upper surface, and $h(x, y, t) = z_{top} - z_{bot}$ is the layer's thickness. Subsequent equations assume that ρ varies only as a function of x, y, and t, such that $\rho = \bar{\rho}$, and also assume that $\bar{\rho}$ of material potentially added to the layer locally equals $\bar{\rho}$ of the layer itself.

[64] Integration of (A1) and (A2) through the layer thickness from its base at $z = z_{bot}$ to its upper surface at $z = z_{top}$ involves use of kinematic boundary conditions that relate $v_z(z_{bot})$ and $v_z(z_{top})$ to the other velocity components at $z = z_{bot}$ and $z = z_{top}$ and to variations in the boundary positions:

$$v_z(z_{bot}) = \frac{\partial z_{bot}}{\partial t} + v_x(z_{bot})\frac{\partial z_{bot}}{\partial x} + v_y(z_{bot})\frac{\partial z_{bot}}{\partial y} + E_{bot}(x, y, t), \tag{A4}$$

$$v_z(z_{top}) = \frac{\partial z_{top}}{\partial t} + v_x(z_{top})\frac{\partial z_{top}}{\partial x} + v_y(z_{top})\frac{\partial z_{top}}{\partial y} + E_{top}(x, y, t). \tag{A5}$$

Here E_{bot} and E_{top} are the z-direction boundary-migration velocities (reckoned positive downward) due to passage of material through the basal surface or upper surface of the layer, respectively. *Gray* [2001] has shown that for (A4) and (A5) to describe mass fluxes through these surfaces exactly, E_{bot} and E_{top} must be multiplied by correction factors that account for local differences between the slopes of z_{bot} and z_{top} and the slopes of the global coordinates, x and y. These correction factors are negligible, however, if $z_{bot}(x, y, t)$ and $z_{top}(x, y, t)$ vary gradually enough to satisfy the conditions $[\partial z_{bot}/\partial x]^2$, $[\partial z_{bot}/\partial y]^2$, $[\partial z_{top}/\partial x]^2$, and $[\partial z_{top}/\partial y]^2 \ll 1$, and here I assume that this is the case. Then (A5) shows that if a static layer with $v_x = v_y = v_z = 0$ is subject to upward surface accretion ($E_{top} < 0$), the deposit's surface height increases at the rate $\partial z_{top}/\partial t = -E_{top}$. The situation is more complicated at the base of a moving layer, where either erosion or sedimentation can occur and all of the terms in (A4) can evolve simultaneously. Despite such complications, $E_{bot} < 0$ always describes upward migration of the layer's base due to sedimentation, and $E_{bot} > 0$ describes basal lowering due to erosion.

[65] Provided that $\rho = \bar{\rho}$, depth integration of the mass-conservation (equation A1) from $z = b$ to $z = \eta$ yields

$$\begin{aligned}
&\int_{z_{bot}}^{z_{top}} \left[\frac{\partial\bar{\rho}}{\partial t} + \frac{\partial(\bar{\rho}v_x)}{\partial x} + \frac{\partial(\bar{\rho}v_y)}{\partial y} + \frac{\partial(\bar{\rho}v_z)}{\partial z}\right]dz \\
&= h\frac{\partial\bar{\rho}}{\partial t} + h\bar{v}_x\frac{\partial\bar{\rho}}{\partial x} + h\bar{v}_y\frac{\partial\bar{\rho}}{\partial y} + \bar{\rho}\left[v_z(z_{top}) - v_z(z_{bot})\right] \\
&+ \bar{\rho}\left[\frac{\partial}{\partial x}\int_{z_{bot}}^{z_{top}} v_x dz - v_x(z_{top})\frac{\partial z_{top}}{\partial x} + v_x(z_{bot})\frac{\partial z_{bot}}{\partial x}\right. \\
&\left. + \frac{\partial}{\partial y}\int_{z_{bot}}^{z_{top}} v_y dz - v_y(z_{top})\frac{\partial z_{top}}{\partial y} v_y(z_{bot})\frac{\partial z_{bot}}{\partial y}\right] \\
&= h\frac{\partial\bar{\rho}}{\partial t} + \frac{\partial(\bar{\rho}h\bar{v}_x)}{\partial x} + \frac{\partial(\bar{\rho}h\bar{v}_y)}{\partial y} \\
&- \bar{\rho}\left[v_x(z_{top})\frac{\partial z_{top}}{\partial x} + v_y(z_{top})\frac{\partial z_{top}}{\partial y} - v_z(z_{top})\right] \\
&+ \bar{\rho}\left[v_x(z_{bot})\frac{\partial z_{top}}{\partial x} + v_y(z_{top})\frac{\partial z_{top}}{\partial y} - v_z(z_{top})\right] \\
&= \frac{\partial(\bar{\rho}h)}{\partial t} + \frac{\partial(\bar{\rho}h\bar{v}_x)}{\partial x} + \frac{\partial(\bar{\rho}h\bar{v}_y)}{\partial y} + \bar{\rho}E_{top} - \bar{\rho}E_{bot} = 0.
\end{aligned} \tag{A6}$$

The third and fourth lines of (A6) illustrate the result of using Leibniz' rule [*Abramowitz and Stegun*, 1964, pp. 11] for interchanging the order of integration and differentiation during evaluation of $\int_{z_{bot}}^{z_{top}}[\partial v_x/\partial x]dz$ and $\int_{z_{bot}}^{z_{top}}[\partial v_y/\partial y]dz$. The final line of (A6) results from substituting the kinematic boundary conditions (A4) and (A5) into the sixth and seventh lines of (A6) in place of $v_z(z_{top})$ and $v_z(z_{bot})$, and then cancelling terms that sum to zero and making the identification $\partial(z_{top} - z_{bot})/\partial t = \partial h/\partial t$. If $\bar{\rho}$ is constant and $E_{top} = E_{bot} = 0$, then (A6) reduces to the standard depth-averaged mass-conservation division used in many shallow-flow theories [e.g., *Vreugdenhil*, 1994; *Pudasaini and Hutter*, 2007].

[66] Depth integration of the momentum-conservation (A2) equation proceeds in a manner similar to that of the mass-conservation equation, and it yields

$$\begin{aligned}
&\int_{z_{bot}}^{z_{top}} \left(\frac{\partial(\rho v_x)}{\partial t} + \frac{\partial(\rho v_x^2)}{\partial x} + \frac{\partial(\rho v_x v_y)}{\partial y} + \frac{\partial(\rho v_x v_z)}{\partial z}\right)dz \\
&= \frac{\partial}{\partial t}\bar{\rho}\int_{z_{bot}}^{z_{top}} v_x dz - \bar{\rho}v_x(z_{top})\frac{\partial z_{top}}{\partial t} + \bar{\rho}v_x(z_{bot})\frac{\partial z_{bot}}{\partial t} \\
&+ \frac{\partial}{\partial x}\bar{\rho}\int_{z_{bot}}^{z_{top}} v_x^2 dz - \bar{\rho}v_x^2(z_{top})\frac{\partial z_{top}}{\partial x} + \bar{\rho}v_x^2(z_{bot})\frac{\partial z_{bot}}{\partial x} \\
&+ \frac{\partial}{\partial y}\bar{\rho}\int_{z_{bot}}^{z_{top}} v_x v_y dz - \bar{\rho}v_x(z_{top})v_y(z_{top})\frac{\partial z_{top}}{\partial y} \\
&+ \bar{\rho}v_x(z_{bot})v_y(z_{bot})\frac{\partial z_{bot}}{\partial y} + \bar{\rho}v_x(z_{top})v_z(z_{top}) - \bar{\rho}v_x(z_{bot})v_z(z_{bot}) \\
&= \frac{\partial(\bar{\rho}h\bar{v}_x)}{\partial t} + \frac{\partial(\bar{\rho}h\bar{v}_x^2)}{\partial x} + \frac{\partial(\bar{\rho}h\bar{v}_x\bar{v}_y)}{\partial y} + \frac{\partial}{\partial x}\bar{\rho}\int_{z_{bot}}^{z_{top}} (v_x - \bar{v}_x)^2 dz \\
&+ \frac{\partial}{\partial y}\bar{\rho}\int_{z_{bot}}^{z_{top}} (v_x - \bar{v}_x)(v_y - \bar{v}_y)dz + \bar{\rho}v_x(z_{top})E_{top} - \bar{\rho}v_x(z_{bot})E_{bot} \\
&= \int_{z_{bot}}^{z_{top}} \Sigma F_x dz.
\end{aligned} \tag{A7}$$

The momentum-exchange terms $\bar{\rho}v_x(z_{top})E_{top}$ and $-\bar{\rho}v_x(z_{bot})E_{bot}$ arise in the seventh line of (A7) as a result of using the kinematic boundary conditions (A4) and (A5) to combine several terms in the second through fifth lines of (A7), which express contributions to the x-momentum fluxes at the flow boundaries. The integrals in the sixth and seventh lines of (A7) result from use of the identities

$$\begin{aligned}
\int_{z_{bot}}^{z_{top}} v_x^2 dz &= h\bar{v}_x^2 + \int_{z_{bot}}^{z_{top}} (v_x - \bar{v}_x)^2 dz \\
\int_{z_{bot}}^{z_{top}} v_x v_y dz &= h\bar{v}_x\bar{v}_y + \int_{z_{bot}}^{z_{top}} (v_x - \bar{v}_x)(v_y - \bar{v}_y)dz,
\end{aligned} \tag{A8}$$

which show how the depth integrals of products are related to the products of depth integrals. Physically, the integrands $(v_x - \bar{v}_x)^2$ and $(v_x - \bar{v}_x)(v_y - \bar{v}_y)$ describe the effects of differential advection of momentum due to variations of v_x and v_y

with z [*Vreugdenhil*, 1994]. Depth-averaged flow theories commonly account for these effects by introducing momentum-distribution coefficients that multiply $h\bar{v}_x^2$ and $h\bar{v}_x\bar{v}_y$, as exemplified by equation (21) in the main text. The one-dimensional depth-averaged conservation laws (19) and (20) in the main text are obtained from (A6) and (A7) by utilizing the momentum distribution coefficient $\beta = (1/h\bar{v}_x^2)\int_{z_{bot}}^{z_{top}} v_x^2 dz$, neglecting all terms involving $\partial/\partial y$, and assuming $\bar{\rho}$ is constant.

Appendix B: Evaluation of Depth-averaged Normal Stresses to Reduce Equation (24) to Equation (26)

[67] If the position of the upper surface of the three-layer system shown in Figure 5 is denoted by $z = H$, then the total normal stress σ_{zz} at any depth $H - z$ below the surface is found by integrating equation (18) to obtain $\sigma_{zz} = \rho g(H - z)\cos\theta$. Furthermore, if at all depths the lateral normal stress σ_{xx} is related to σ_{zz} by a simple proportionality rule, $\sigma_{xx} = \kappa\sigma_{zz}$ (where κ can be interpreted as a lateral earth-pressure coefficient or elastic Poisson's ratio), then

$$\sigma_{xx} = \kappa\rho g(H - z)\cos\theta. \tag{B1}$$

In the equations that follow, κ is assumed constant within any particular layer, although its value may differ between layers.

[68] The thickness of any layer is given by

$$h = z_{top} - z_{bot}, \tag{B2}$$

and (B1) implies that the depth-averaged lateral normal stress within any layer is given by

$$\bar{\sigma}_{xx} = \frac{\sigma_{xxtop} + \sigma_{xxbot}}{2} = \kappa\rho g\cos\theta\left[H - \frac{z_{top} + z_{bot}}{2}\right]. \tag{B3}$$

Use of (B2) and (B3) and some algebraic rearrangement then enables the product $\bar{\sigma}_{xx}h$, which appears in (24), to be written as

$$\bar{\sigma}_{xx}h = \kappa\rho g\cos\theta\left[H(z_{top} - z_{bot}) - \frac{1}{2}\left({z_{top}}^2 - {z_{bot}}^2\right)\right]. \tag{B4}$$

Differentiation of (B4) with respect to x, followed by some further algebraic rearrangement, then yields a useful form of one of the terms in (24):

$$-\frac{\partial(\bar{\sigma}_{xx}h)}{\partial x} = -\kappa\rho g\cos\theta\left[(z_{top} - z_{bot})\frac{\partial H}{\partial x} + (H - z_{top})\frac{\partial z_{top}}{\partial x} - (H - z_{bot})\frac{\partial z_{bot}}{\partial x}\right]. \tag{B5}$$

Two other terms in (24) can be evaluated directly through use of (B1) to obtain

$$\sigma_{xxtop}\frac{\partial z_{top}}{\partial x} = \kappa\rho g\cos\theta(H - z_{top})\frac{\partial z_{top}}{\partial x}, \tag{B6}$$

$$-\sigma_{xxbot}\frac{\partial z_{bot}}{\partial x} = -\kappa\rho g\cos\theta(H - z_{bot})\frac{\partial z_{bot}}{\partial x}. \tag{B7}$$

Addition of (B5), (B6) and (B7), followed by some algebraic cancellations and use of the substitution $z_{top} - z_{bot} = h$, then shows that this combination of terms reduces to

$$-\frac{\partial(\bar{\sigma}_{xx}h)}{\partial x} + \sigma_{xxtop}\frac{\partial z_{top}}{\partial x} - \sigma_{xxbot}\frac{\partial z_{bot}}{\partial x} = -\kappa\rho gh\cos\theta\frac{\partial H}{\partial x}. \tag{B8}$$

Therefore, provided that equation (B1) is valid and κ is constant within any particular layer, substitution of (B8) in equation (24) reduces it to equation (26).

[69] **Acknowledgments.** I thank Christophe Ancey, Mark Schmeeckle, Nico Gray, Jason Kean, and Mark Reid for useful discussions and comments on a draft manuscript. Scott McCoy and his coauthors cordially provided access to their results from field monitoring at the Chalk Cliffs site in Colorado. I especially thank numerous colleagues who participated in USGS debris-flow flume experiments that helped motivate this work.

References

Abele, G. (1997), Rockslide movement supported by the mobilization of groundwater-saturated valley floor sediments, *Z. Geomorphol.*, *41*, 1–20.

Abramowitz, M., and I. A. Stegun (eds.) (1964), *Handbook of Mathematical Functions with Formulas, Graphs, and Mathematical Tables*, U.S. Dept. of Commer. Natl. Bur. Stand., Washington, D. C.

Armanini, A., H. Capart, L. Fraccarollo, and M. Larcher (2005), Rheological stratification in experimental free-surface flows of granular-liquid mixtures, *J. Fluid Mech.*, *532*, 269–319, doi:10.1017/S0022112005004283.

Armanini, A., L. Fraccarollo, and G. Rosatti (2009), Two-dimensional simulation of debris flows in erodible channels, *Comput. Geosci.*, *35*, 993–1006, doi:10.1016/j.cageo.2007.11.008.

Bear, J. (1972), *Dynamics of Fluids in Porous Media*, Elsevier, New York.

Benda, L. (1990), The influence of debris flows on channels and valley floors in the Oregon Coast Range, USA, *Earth Surf. Processes Landforms*, *15*, 457–466, doi:10.1002/esp.3290150508.

Berger, C., B. W. McArdell, and F. Schlunegger (2011), Direct measurement of channel erosion by debris flows, Illgraben, Switzerland, *J. Geophys. Res.*, *116*, F01002, doi:10.1029/2010JF001722.

Berti, M., R. Genevois, A. Simoni, and P. Rosella Tecca (1999), Field observations of a debris flow event in the Dolomites, *Geomorphology*, *29*, 265–274, doi:10.1016/S0169-555X(99)00018-5.

Berzi, D., J. T. Jenkins, and M. Larcher (2010), Debris flows: Recent advances in experiments and modeling, *Adv. Geophys.*, *52*, 103–138, doi:10.1016/S0065-2687(10)52002-8.

Bouchut, F., E. D. Fernandez-Nieto, A. Mangeney, and P.-Y. Lagrée (2008), On new erosion models of Savage-Hutter type for avalanches, *Acta Mech.*, *227*, 7720–7754, doi:10.1007/s00707-007-0534-9.

Boyer, F., E. Guazzelli, and O. Pouliquen (2011), Unifying suspension and granular rheology, *Phys. Rev. Lett.*, *107*, 188301, doi:10.1103/PhysRevLett.107.188301.

Breien, H., F. V. De Blasio, A. Elverhøi, and K. Høeg (2008), Erosion and morphology of a debris flow caused by a glacial lake outburst flood, western Norway, *Landslides*, *5*, 271–280, doi:10.1007/s10346-008-0118-3.

Brufau, P., P. Garcia-Navarro, P. Ghilardi, L. Natale, and F. Savi (2000), 1-D Mathematical modelling of debris flow, *J. Hydraul. Res.*, *38*, 435–446, doi:10.1080/00221680009498297.

Cannon, S. H., and W. Z. Savage (1988), A mass-change model for the estimation of debris flow runout, *J. Geol.*, *96*, 221–227, doi:10.1086/629211.

Chadwick, P. (1976), *Continuum Mechanics: Concise Theory and Problems*, Wiley, New York.

Chen, H., G. B. Crosta, and C. F. Lee (2006), Erosional effects on runout of fast landslides, debris flows and avalanches: A numerical investigation, *Geotechnique*, *56*, 305–322, doi:10.1680/geot.2006.56.5.305.

Coe, J. A., D. A. Kinner, and J. W. Godt (2008), Initiation conditions for debris flows generated by runoff at Chalk Cliffs, central Colorado, *Geomorphology*, *96*, 270–297, doi:10.1016/j.geomorph.2007.03.017.

Crosta, G. B., S. Imposimato, and D. Roddeman (2009a), Numerical modelling of entrainment/deposition in rock and debris-avalanches, *Eng. Geol. Amsterdam*, *109*, 135–145, doi:10.1016/j.enggeo.2008.10.004.

Crosta, G. B., S. Imposimato, and D. Roddeman (2009b), Numerical modeling of 2-D granular step collapse on erodible and nonerodible surface, *J. Geophys. Res.*, *114*, F03020, doi:10.1029/2008JF001186.

Denlinger, R. P., and R. M. Iverson (2001), Flow of variably fluidized granular masses across three-dimensional terrain: 2. Numerical predictions

and experimental tests, *J. Geophys. Res.*, *106*, 553–566, doi:10.1029/2000JB900330.

Denlinger, R. P., and R. M. Iverson (2004), Granular avalanches across irregular three-dimensional terrain: 1. Theory and Computation, *J. Geophys. Res.*, *109*, F01014, doi:10.1029/2003JF000085.

Doyle, E. E., S. J. Cronin, and J.-C. Thouret (2011), Defining conditions for bulking and debulking of lahars, *Geol. Soc. Am. Bull.*, *123*, 1234–1246, doi:10.1130/B30227.1.

Egashira, S., N. Honda, and T. Itoh (2001), Experimental study on the entrainment of bed material into debris flow, *Phys. Chem. Earth*, *26*, 645–650.

Erlichson, H. (1991), A mass-change model for the estimation of debris-flow runout, A second discussion: Conditions for the application of the rocket equation, *J. Geol.*, *99*, 633–634, doi:10.1086/629522.

Fagents, S. M., and S. A. Baloga (2006), Toward a model for the bulking and debulking of lahars, *J. Geophys. Res.*, *111*, B10201, doi:10.1029/2005JB003986.

Forterre, Y., and O. Pouliquen (2008), Flows of dense granular media, *Annu. Rev. Fluid Mech.*, *40*, 1–24, doi:10.1146/annurev.fluid.40.111406.102142.

Fraccarollo, L., and H. Capart (2002), Riemann wave description of erosional dam-break flows, *J. Fluid Mech.*, *461*, 183–228, doi:10.1017/S0022112002008455.

Freeze, R. A., and J. A. Cherry (1979), *Groundwater*, Prentice-Hall, Englewood Cliffs, N. J.

George, D. L., and R. M. Iverson (2011), A two-phase debris-flow model that includes coupled evolution of volume fractions, granular dilatancy, and pore-fluid pressure, in *Debris-flow Hazards Mitigation, Mechanics, Prediction, and Assessment*, edited by R. Genevois, D. L. Hamilton, and A. Prestininzi, pp. 367–374, Casa Editrice Univ. La Sapienza, Rome.

Godt, J. W., and J. A. Coe (2007), Alpine debris flows triggered by a 28 July 1999 thunderstorm in the central Front Range, Colorado, *Geomorphology*, *84*, 80–97, doi:10.1016/j.geomorph.2006.07.009.

Gray, J. M. N. T. (2001), Granular flow in partially filled slowly rotating drums, *J. Fluid Mech.*, *441*, 1–29, doi:10.1017/S0022112001004736.

Heim, A. (1932), *Bergsturz und Menschenleben* [in German], Naurforschenden Gesellschaft, Zurich, Switzerland. [English translation, BiTech Publ., Vancouver, Canada, 1989.]

Hungr, O. (1990), Momentum transfer and friction in the debris of rock avalanches: Discussion, *Can. Geotech. J.*, *27*, 697, doi:10.1139/t90-083.

Hungr, O., and S. G. Evans (2004), Entrainment of debris in rock avalanches: An analysis of a long run-out mechanism, *Geol. Soc. Am. Bull.*, *116*, 1240–1252, doi:10.1130/B25362.1.

Hungr, O., G. C. Morgan, and R. Kellerhals (1984), Quantitative analysis of debris torrent hazards for design of remedial measures, *Can. Geotech. J.*, *21*, 663–677, doi:10.1139/t84-073.

Hungr, O., S. McDougall, and M. Bovis (2005), Entrainment of material by debris flows, in *Debris-flow Hazards and Related Phenomena*, edited by M. Jakob and O. Hungr, pp. 135–158, Springer, Chichester, U. K., doi:10.1007/3-540-27129-5_7.

Hutchinson, J. N., and R. K. Bhandari (1971), Undrained loading, a fundamental mechanism of mudflows and other mass movements, *Geotechnique*, *21*, 353–358, doi:10.1680/geot.1971.21.4.353.

Iverson, R. M. (1997), The physics of debris flows, *Rev. Geophys.*, *35*, 245–296, doi:10.1029/97RG00426.

Iverson, R. M. (2005), Debris-flow mechanics, in *Debris-Flow Hazards and Related Phenomena*, edited by M. Jakob and O. Hungr, pp. 105–134, Springer, Chichester, U. K., doi:10.1007/3-540-27129-5_6.

Iverson, R. M. (2009), Elements of an improved model of debris-flow motion, in *Powders and Grains 2009 (Proceedings of the Sixth International Conference on Micromechanics of Granular Media)*, edited by M. Nakagawa and S. Luding, pp. 9–16, Am. Inst. of Phys., Melville, New York.

Iverson, R. M., and R. P. Denlinger (2001), Flow of variably fluidized granular masses across three-dimensional terrain: 1. Coulomb mixture theory, *J. Geophys. Res.*, *106*, 537–552, doi:10.1029/2000JB900329.

Iverson, R. M., and R. G. LaHusen (1989), Dynamic pore-pressure fluctuations in rapidly shearing granular materials, *Science*, *246*, 796–799, doi:10.1126/science.246.4931.796.

Iverson, R. M., M. E. Reid, and R. G. LaHusen (1997), Debris-flow mobilization from landslides, *Annu. Rev. Earth Planet. Sci.*, *25*, 85–138, doi:10.1146/annurev.earth.25.1.85.

Iverson, R. M., M. Logan, R. G. LaHusen, and M. Berti (2010), The perfect debris flow? aggregated results from 28 large-scale experiments, *J. Geophys. Res.*, *115*, F03005, doi:10.1029/2009JF001514.

Iverson, R. M., M. E. Reid, M. Logan, R. G. LaHusen, J. W. Godt, and J. G. Griswold (2011), Positive feedback and momentum growth during debris-flow entrainment of wet bed sediment, *Nat. Geosci.*, *4*, 116–121, doi:10.1038/ngeo1040.

Jaeger, J. C. (1969), *Elasticity, Fracture and Flow, with Engineering and Geological Applications*, Chapman and Hall, London.

Johnson, C. G., B. P. Kokelaar, R. M. Iverson, M. Logan, R. G. LaHusen, and J. M. N. T. Gray (2012), Grain-size segregation and levee formation in geophysical mass flows, *J. Geophys. Res.*, *117*, F01032, doi:10.1029/2011JF002185.

Komatsu, T. S., S. Inagaki, N. Nakagawa, and S. Nasuno (2001), Creep motion in a granular pile exhibiting steady surface flow, *Phys. Rev. Lett.*, *86*, 1757–1760, doi:10.1103/PhysRevLett.86.1757.

Lade, P. V., and R. De Boer (1997), The concept of effective stress for soil, concrete and rock, *Geotechnique*, *47*, 61–78, doi:10.1680/geot.1997.47.1.61.

Lambe, T. W., and R. V. Whitman (1979), *Soil Mechanics, SI Version*, Wiley, New York.

Larcher, M., L. Fraccarollo, A. Armanini, and H. Capart (2007), Set of measurement data from flume experiments on steady uniform debris flows, *J. Hydraul. Res.*, *45*, 59–71, doi:10.1080/00221686.2007.9521833.

Le, L., and E. B. Pitman (2010), A model for granular flows over an erodible surface, *SIAM J. Appl. Math.*, *70*, 1407–1427, doi:10.1137/060677501.

Malvern, L. E. (1969), *Introduction to the Mechanics of a Continuous Medium*, Prentice-Hall, Englewood Cliffs, New Jersey.

Mangeney, A., L. S. Tsimring, D. Volfson, I. S. Aranson, and F. Bouchut (2007), Avalanche mobility induced by the presence of an erodible bed and associated entrainment, *Geophys. Res. Lett.*, *34*, L22401, doi:10.1029/2007GL031348.

Mangeney, A., O. Roche, O. Hungr, N. Mangold, G. Faccanoni, and A. Lucas (2010), Erosion and mobility in granular collapse over sloping beds, *J. Geophys. Res.*, *115*, F03040, doi:10.1029/2009JF001462.

McCoy, S. W., J. W. Kean, J. A. Coe, D. M. Staley, T. A. Wasklewicz, and G. E. Tucker (2010), Evolution of a natural debris flow: In situ measurements of flow dynamics, video imagery, and terrestrial laser scanning, *Geology*, *38*, 735–738, doi:10.1130/G30928.1.

McDougall, S., and O. Hungr (2005), Dynamic modelling of entrainment in rapid landslides, *Can. Geotech. J.*, *42*, 1437–1448, doi:10.1139/t05-064.

MiDi GDR Group (2004), On dense granular flows, *Eur. Phys. J. E*, *14*, 127–135.

Papa, M., S. Egashira, and T. Itoh (2004), Critical conditions of bed sediment entrainment due to debris flow, *Nat. Hazards Earth Syst. Sci.*, *4*, 469–474, doi:10.5194/nhess-4-469-2004.

Pierson, T. C. (1980), Erosion and deposition by debris flows at Mt. Thomas, North Canterbury, New Zealand, *Earth Surf. Processes*, *5*, 227–247.

Pierson, T. C., R. J. Janda, J.-C. Thouret, and C. A. Borrero (1990), Perturbation and melting of snow and ice by the 13 November 1985 eruption of Nevado del Ruiz, Colombia, and consequent mobilization, flow and deposition of lahars, *J. Volcanol. Geotherm. Res.*, *41*, 17–66, doi:10.1016/0377-0273(90)90082-Q.

Pitman, E. B., C. C. Nichita, A. K. Patra, A. C. Bauer, M. Bursik, and A. Webb (2003), A model of granular flows over an erodible surface, *Discrete Contin. Dyn. Syst.*, *3*, 589–599, doi:10.3934/dcdsb.2003.3.589.

Pudasaini, S. P., and K. Hutter (2007), *Avalanche Dynamics*, Springer, Berlin.

Reid, M. E., R. M. Iverson, M. Logan, R. G. LaHusen, J. W. Godt, and J. G. Griswold (2011), Entrainment of bed sediment by debris flows: Results from large-scale experiments, in *Debris-flow Hazards Mitigation, Mechanics, Prediction, and Assessment*, edited by R. Genevois, D. L. Hamilton, and A. Prestininzi, pp. 367–374, Casa Editrice Univ. La Sapienza, Rome.

Rice, J. R., and M. P. Cleary (1976), Some basic stress diffusion solutions for fluid-saturated elastic porous media with compressible constituents, *Rev. Geophys.*, *14*, 227–241, doi:10.1029/RG014i002p00227.

Rickenmann, D., D. Weber, and B. Stepanov (2003), Erosion by debris flows in field and laboratory experiments, in *Debris-flow Hazards Mitigation, Mechanics, Prediction, and Assessment*, edited by D. Rickenmann and C.-L. Chen, pp. 883–894, Millpress, Rotterdam, Netherlands.

Rudnicki, J. W. (1984), Effects of dilatant hardening on the development of concentrated shear deformation in fissured rock masses, *J. Geophys. Res.*, *89*, 9259–9270, doi:10.1029/JB089iB11p09259.

Sassa, K. (1985), The mechanism of debris flows, in *Proceedings of the Eleventh International Conference on Soil Mechanics and Foundation Engineering*, pp. 1173–1176, Balkema, Rotterdam, Netherlands.

Schofield, A. N., and P. Wroth (1968), *Critical State Soil Mechanics*, McGraw-Hill, New York.

Scott, K. M., J. W. Vallance, N. Kerle, J. L. Macias, W. Strauch, and G. Devoli (2005), Catastrophic precipitation-triggered lahar at Casita volcano, Nicaragua: Occurrence, bulking and transformation, *Earth Surf. Processes Landforms*, *30*, 59–79, doi:10.1002/esp.1127.

Skempton, A. W. (1954), The pore pressure coefficients A and B, *Geotechnique*, *4*, 143–147, doi:10.1680/geot.1954.4.4.143.

Sovilla, B., P. Burlando, and P. Bartelt (2006), Field experiments and numerical modeling of mass entrainment in snow avalanches, *J. Geophys. Res.*, *111*, F03007, doi:10.1029/2005JF000391.

Stiny, J. (1910), *Die Muren (Debris Flows)* [in German], Wagnerschen Univ., Buchhandlung, Innsbruck, Austria. [English translation, EBA Consult., Vancouver, Canada, 1997.]

Tai, Y. C., and C. Y. Kuo (2008), A new model of granular flows over general topography with erosion and deposition, *Acta Mech.*, *199*, 71–96, doi:10.1007/s00707-007-0560-7.

Takahashi, T. (1978), Mechanical characteristics of debris flow, *J. Hydraul. Div. Am. Soc. Civ. Eng.*, *104*, 1153–1169.

Takahashi, T. (1991), *Debris Flow*, Balkema, Rotterdam, Netherlands.

Van Gassen, W., and D. M. Cruden (1989), Momentum transfer and friction in the debris of rock avalanches, *Can. Geotech. J.*, *26*, 623–628, doi:10.1139/t89-075.

Vanoni, V. A. (Ed.) (1975), *Sedimentation Engineering*, Am. Soc. of Civ. Eng., New York.

Voight, B., and J. Sousa (1994), Lessons from Ontake-san: A comparative analysis of debris avalanche dynamics, *Eng. Geol. Amsterdam*, *38*, 261–297, doi:10.1016/0013-7952(94)90042-6.

Vreugdenhil, C. B. (1994), *Numerical Methods for Shallow-Water Flow*, Kluwer, Dordrecht, Netherlands.

Wang, G., K. Sassa, and H. Fukuoka (2003), Downslope volume enlargement of a debris slide-debris flow in the 1999 Hiroshima, Japan, rainstorm, *Eng. Geol. Amsterdam*, *69*, 309–330, doi:10.1016/S0013-7952(02)00289-2.